CORRELATING THERMAL PROPERTIES OF SPUTTERED TANTALUM AND TANTALUM NITRIDE THIN FILMS OF VARYING N_2 CONTENT WITH MECHANICAL, ELECTRICAL AND STRUCTURAL PROPERTIES

A Thesis

Presented to the Faculty of the Graduate School

of Cornell University

In Partial Fulfillment of the Requirements for the Degree of

Master of Science

by

Tasnuva Tabassum

August 2017

ABSTRACT

With rapid growth in the semiconductor industry, the need for optimization of nanofabrication processes is ever increasing. In such processes, TaN films are of great interest as they create effective diffusion barriers against Cu interconnects in integrated circuits. These circuits may be subjected to elevated temperatures during processing and it is important to study the changes in properties of materials involved. Surprisingly, limited data on the constant pressure specific heat capacity (c_p) of Ta and TaN thin films exist. This thesis studies the changes in c_p from room temperature to 400°C of sputter-deposited Ta and TaN thin films with varied N_2 partial pressure. Parallel studies of mechanical, electrical and structural changes are conducted on as-deposited and annealed samples to correlate to changes in c_p. The c_p of films increases with temperature, as seen in bulk forms of Ta and TaN. Low temperature resistivity measurements are performed to study the effect of lattice vibrations decreasing. The electrical properties of TaN, deposited in greater than 23% N_2 content, are found to be insulating. Annealing decreases the resistivity of Ta films which is attributed to defect healing. The hardness and Young's modulus increase up to 27% N_2 content of TaN films. The residual stress in these films range from highly tensile Ta to increasingly compressive TaN with increased N_2 content. The TaN film with the lowest inducing stress was 18% N_2 with a compressive stress of -5.82 MPa.

BIOGRAPHICAL SKETCH

The author, Tasnuva Tabassum, was born in Dhaka, Bangladesh and grew up right in the heart of the city. She completed her primary and secondary education from Scholastica Private Ltd. To pursue further education, she moved to London, UK where she obtained a Bachelor of Engineering degree in Materials Science and Engineering at Queen Mary University of London. During her final year, she worked with late Senior Lecturer, Dr. Russell Binions, on his research on 'Thermochromic Thin Films for Architectural Applications'. Upon graduation, she moved to US and worked at PNC Bank NA as a Financial Consultant to save up for graduate studies. In Fall 2015, she started her Masters of Science degree at Cornell University where she started working on an industrial project sponsored by Applied Materials Inc. (AMAT).She performed research for the company using Cornell Nanoscale Science & Technology Facility (CNF) and Cornell Center for Materials Research (CCMR) facilities under the guidance of Professor Robert B. van Dover, Professor Emeritus Dieter Ast, David Lynch, Dr. Mats Larsson and Kevin Papke (last 2 mentors from AMAT). During her 2nd year at Cornell, she spent 6 months at AMAT headquarters in Santa Clara, CA developing from scratch, an automated version of one of the company's coating test methods. She has obtained a patent on this novel method as first inventor with Dr. Mats Larsson and Kevin Papke as 2nd and 3rd inventors respectively. She then returned to Cornell University in January 2017 to work extensively on her research in 'Thermal Properties of Tantalum and Tantalum Nitride Thin Films'. Upon graduation in July 2017, she joined AMAT as a Process Engineer in Kevin Papke's 'Surface Technology' group in Applied Global Services (AGS).

DEDICATION

Dedicated to my parents, of course, for everything.

To my elder brother, Shafi, who inspired me to be independent, strong, and ruthless through very unhealthy competition.

To my 1-year old nephew, Zayyan, who is oceans away in the depths of Bedfordshire, but the closest to my heart. I hope to inspire you some day.

To my best friend, Prom, for being there since as far as I can remember. Thank you for making me feel better about procrastinating.

To Professor Ast for seeing things in me that I didn't see myself.

And finally, thank you god, if you are up there somewhere.

ACKNOWLEDGMENTS

Firstly, I would like to express my sincere gratitude towards my graduate committee members: Professor Robert B. van Dover, Professor Dieter Ast and Professor Stuart L. Phoenix for their innovative ideas, creativity, encouragement, and for having an answer to all my problems. Thank you, especially to Professor van Dover, for allowing me to conduct research on an industrial project, in place of his own research interests. Thank you for allowing me to leave campus for six months for an AMAT project, and for finding the time to meet with me thrice a week despite having an extraordinarily busy schedule. I truly mean it when I say that I couldn't have made a better choice when I chose you as my primary advisor after speaking to 6 other advisors in the department. Your sincere interest in my growth and your humility inspires me to be a better person and leader.

Professor Dieter Ast, thank you for having every possible solution to all the dilemmas I have faced, both during research and in my career. You have time and time again proved your sincere enthusiasm in my success by sending out literature papers, useful articles and emails with invaluable advice that I will hold close to my heart for years to come. The knowledge you have is invaluable and irreplaceable and I will always look to you for support and guidance. I have realized my true potential through you and only you have made me come to realize that if I set my heart to it, the sky is the limit. You also taught me that 'success is when opportunity meets preparedness' and that I don't need to be the smartest person in the room to be most successful. I just need to outwork them all.

Thank you, Professor Stuart L. Phoenix, for your unique insights, not just on my research, but on other worldly issues. Thank you for adding a diverse experience to my semiconductor background by enlightening me about the complex nature of composites.

Thank you Mats Larsson and Kevin Papke for trusting me with all the responsibilities so far. It would not have been possible to show my true potential otherwise. Thank you and AMAT for sponsoring the last semester of my research. Finally, thank you for letting me explore my creative side by designing a product from scratch for AMAT during my internship. I hope to exceed your expectations as I start my new position at AMAT.

Thank you Joseph Carloni for helping me with obtaining nanoindentation data on my thin films and of course, for your general guidance and challenging questions. David Lynch, I truly appreciate your help when I was a new student and clueless, and for treating me like a peer all along the way. Your sociability is endearing and knowledge, astounding. I have no doubt you will go places and I will always look up to you as inspiration.

Sincere gratitude towards CNF facilities. Tom Pennell, thank you for changing targets in the sputter tool on such short notice and for all the Bosch etching advice; Amrita Banerjee, thank you for helping me find those nano-scratches through SEM; Jerry Drumheller thank you for helping me acquire FleXus scans on very thick Aluminum coupons; Chris Alpha thank you for making CNF fun and for helping out with the KOH hood, Photolithography advice and Zygo; Aaron Windsor thank you for help with Alumina and Si_3N_4 deposition; and last but not least, Director of CNF, Don Tennant, for being so open minded about the new recipes we wanted to introduce to some of your tools. The AMAT project would not have made such significant progress without you and we hope to continue building this relationship in the future.

Thank you to CCMR facilities. Especially Dr. Maura Susan Weathers for assisting me with temperature variable X-ray Diffraction (XRD) scans, Don Werder for help with Energy Dispersive Spectroscopy (EDS), John Grazul for polishing samples himself for me on very

short notice and, of course, being one of the most interesting people I have met so far at Cornell.

I would also like to thank Michele Conrad, former Graduate Field Assistant, for always helping me out with my issues, no matter how minor, and those wonderful conversations where we shared our passion for baking. You are one of the loveliest people I have met so far.

Finally, thank you Cornell University for accepting me. You are the reason I am where I am and will be in the future. I truly felt like I belonged here, despite having imposter syndrome like everyone else. Cornell will always be home to me.

Table of Contents

LIST OF FIGURES

LIST OF TABLES

LIST OF ABBREVIATIONS AND SYMBOLS

Ta: tantalum
TaN: tantalum nitride
N_2: Nitrogen gas
Ar: argon
Cu: copper
Si: silicon
c_p: specific heat capacity at constant pressure
°C: degree Celsius
c_v : specific heat capacity at constant volume
θ_D: Debye temperature
MPa: Mega Pascal (10^6 Pa)
GPa: Giga Pascal (10^9 Pa)
nm: nanometer (10^{-9} m)
J: Joules
g: grams
cNm: centi Newton-meter
K: Kelvin
R: universal gas constant = 8.314 J / mol. K
μΩ: micro-ohm (10^{-6} ohm)
cm: centimeter (10^{-2} m)
mW: milliwatts (1 mJ s^{-1})
A: ampere
V: voltage
DC: direct current
H: hardness
E: Young's modulus
A_C: contact area
h_c: contact depth
E_R: reduced modulus
E_i: Young's modulus of indenter
v_i: Poisson's ratio of indenter
v_s: Poisson's ratio of sample
N: newton
RMS: root-mean squared
σ: stress (in MPa)
t_s: thickness of substrate
t_f: thickness of film
R_o: radius of curvature before deposition (in Flexus)
R: radius of curvature after deposition (in Flexus)
atm: atmospheric pressure
ρ: resistivity (μΩ.cm)
R: resistance (Ω)

R_S: sheet resistance (Ω/sq)
US: ultrasonic force (mW)
AMAT: Applied Materials Inc.
CNF: Cornell Nanoscale Facility
CCMR: Cornell Center for Materials Research
AGS: Applied Global Services
DSC: Differential scanning calorimetry
EDS: energy dispersive spectroscopy
XRD: X-ray Diffraction
SEM: scanning electron microscopy
XPS: X-ray photoelectron spectroscopy
AFM: atomic force microscopy
ALD: atomic layer deposition
PVD: physical vapor deposition
PPMS: physical property measurement system
GMR: Giant magnetoresistance
RF: radio frequency
DC: direct current
GADDS: general area detector diffraction system
HCP: hexagonal close packed
BCC: body centered cubic
FCC: face centered cubic
APF: atomic packing factor
V_P: volume of one atom
V_C: volume of one unit cell
sccm: standard cubic centimeter per minute (gas flow)
LOR: lift off resist
RPM: revolutions per minute
IPA: isopropyl alcohol
PR: photoresist

CHAPTER 1

INTRODUCTION

This thesis is primarily a study of the thermal properties of tantalum (Ta) and tantalum nitride (TaN) thin films as a function of temperature, and correlating changes in structural, mechanical and electrical properties as a result of varying temperature and nitrogen (N_2) content (for the TaN films) by changing N_2 partial pressure during sputter deposition.

Introduction to Applications of Tantalum and Tantalum Nitride films in the Semiconductor Industry

The semiconductor industry is not only a crucial aspect for the economic growth of the electronics industry, but to a significant extent, determines the speed at which innovation in technology occurs. With rapid growth in technology, the need for optimization of nanofabrication processes is ever increasing. Academic and industrial organizations are in constant competition with each other to produce the best combination of materials and processes in terms of speed, cost effectiveness, and energy efficiency.

To increase areal density, the focus of the semiconductor industry has largely been on compacting and miniaturizing components on an integrated circuit. To achieve this, very thin layers of material films, in the range of nanometers (nm), are possible to deposit and pattern to make interconnects on the nanoscale on a semiconductor material acting as the substrate.

Ta and TaN thin films are of interest in the semiconductor industry as they act as an impenetrable diffusion barrier for copper (Cu) interconnects made on these integrated

circuits. TaN has been found to exhibit better diffusion barrier properties than the pure metal form. If not for such diffusion barriers, the high diffusivity of Cu in silicon (Si) and other materials on integrated circuits could lead to device failure through current leakage [1, 2, 3]. TaN thin films are also widely used for thin film resistors, which make their electrical properties another important focus for research [4].

Aim of Study

In the nanofabrication processes described above, the microchips with Ta and TaN films may very well be subjected to elevated temperatures. The thermal properties of these films are therefore investigated in detail and correlated to changes in structure, electrical resistivity and mechanical properties. Limited data exists on the specific heat capacity at constant pressure, c_p, of Ta and TaN films, and therefore this study will focus primarily on this property.

More recently, atomic layer deposition (ALD) for diffusion barriers is preferred due to great conformity, uniformity and minimal thickness [5]. However, this study will be focused on films deposited via a (reactive) sputtering physical vapor deposition (PVD) method due to availability of tools, cost effectiveness and speed of deposition. Sputter deposition is also easily manipulative in terms of N_2 content in films and is therefore preferable for this study where the effect of N_2 content is a primal focus. For diffusion barriers, uniformity of sputter deposited films, thickness control and residual stresses are also useful parameters to study.

Introduction to Properties of Tantalum and Tantalum Nitride films from Literature Review

Additional properties which make TaN films especially attractive in the semiconductor industry is their chemical inertness, and stable thermal and electrical properties. The mechanical hardness of these films is ideal for applications such as wear resistant coatings [6]. The variability in electrical resistance and mechanical properties of TaN films, through deposition conditions, also make them flexible for various applications. For example, for diffusion barriers mentioned above, low resistivity is preferred to minimize electrical resistance whereas in other applications such as for the seeding layer in giant magnetoresistance (GMR) sensors, high resistivity TaN films reduce eddy current loss [3, 7].

There is currently very limited research on the specific heat capacities and the temperature dependence of this property for Ta and TaN thin films. Literature values for bulk tantalum have been reported to be about 0.142 J g^{-1} K^{-1} at room temperature (300 K) to about 0.148 J g^{-1} K^{-1} at 700 K (427 °C) [8]. The bulk value for specific heat capacity at room temperature for TaN has been found to be 0.210 J g^{-1} K^{-1} [9], which agrees well with other metal nitrides

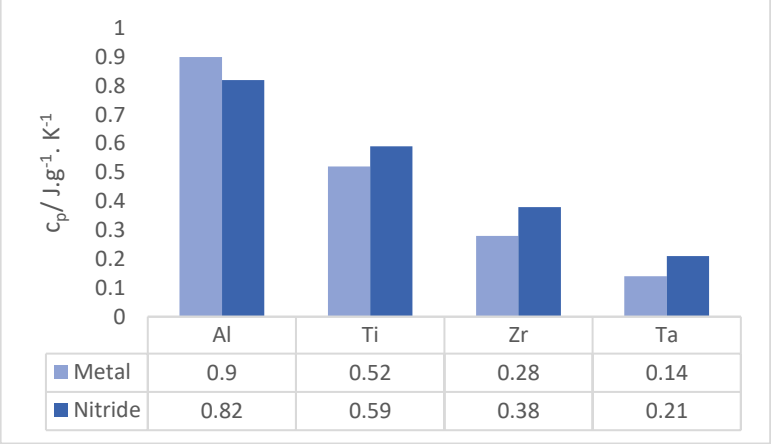

	Al	Ti	Zr	Ta
Metal	0.9	0.52	0.28	0.14
Nitride	0.82	0.59	0.38	0.21

Figure 1: Specific heat capacities at constant pressure of metals and their nitrides [9]

having higher heat capacities than the pure metal states as shown in Figure 1 on previous page.

Specific heat capacities of thin film metals can be higher compared to their bulk values as shown in literature for Al thin films compared to bulk Al. This increase depends on the thickness of the thin film deposited as shown in literature [10]. The change in c_p of Ta and TaN according to Debye saturation model (Dulong-Petit Law) has been studied where the Debye temperature of Ta is 230 K. This means, according to the Dulong-Petit Law, the c_p, is not expected to change from room temperature to about 2300K by more than 30%. However, it has been observed in literature, that Ta surpasses these predictions at high temperatures [8].

The Dulong-Petit Law also discovered that the heat capacity of a mole of most solid elements equaled to a constant value of 3*R*, where *R* is universal gas constant and equivalent to 8.314 J / mol. K [11]. This trend is clearly shown on Figure 2 below where, if the c_p is multiplied by the atomic mass, a constant value is obtained.

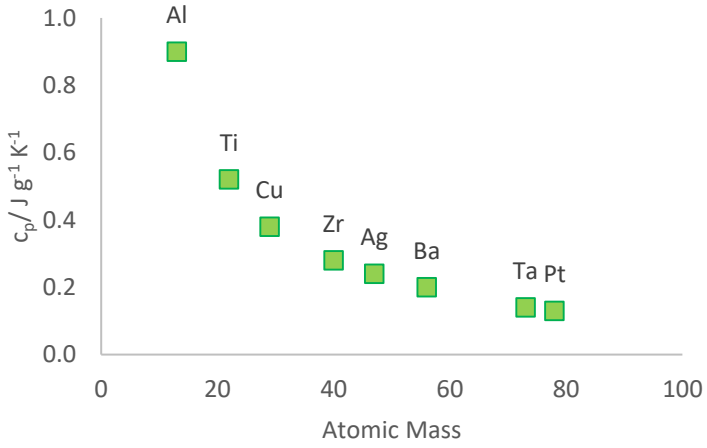

Figure 2: Trend in specific heat capacity at constant pressure as a function of atomic mass [11]

It has been seen in literature that the resistivity of Ta and TaN thin films fall in the range of 10^{-4} μΩ.cm, which falls on the border between a conducting and semiconductor material. The resistivity of TaN films increases with increased Nitrogen content [12, 13, 14]. The temperature dependence of amorphous e-beam (electron beam) evaporated Ta thin films decreases with increasing temperature in various literature [15,16]. The electrical resistivity will be discussed in further detail in chapter 3.

When it comes to the mechanical properties of TaN, the hardness of these films range between 10-18 GPa depending on the N_2 to argon (Ar) ratio. It has been seen in literature that the increased N_2 content gives rise to increased hardness up to about 50% N_2 and falls thereafter [13]. There is no clear trend in the mechanical properties and this is a result of complex changes in structures [12]. Vacuum annealing TaN films has also shown increased hardness (H) apparently due to an effect from enhanced film density [14]. The Young's modulus (E) of TaN films ranges from 150-250 GPa [17]. Vacuum annealing has also shown to increase the E of these thin films, attributing this behavior to a decrease in defect concentration [14].

Deposition rates have shown consistent results of declining with increased N_2 pressure [12, 14] and while some literature with reactive sputtering show that roughness of films generally increase with increasing N_2 [18], other literature where films are deposited via a reactive radio frequency (RF) magnetron sputtering method displays no clear trend [19]. These properties and processes will be discussed in further detail below.

Introduction to Mechanisms and Theory for Equipment Used for Measurements:

1. *Physical Vapor Deposition of Ta and TaN films using AJA Sputter Deposition Tool in CNF*

Sputter deposition is a PVD method of thin film deposition. This process involves ejecting material from a "target" that is a source (Ta) onto a "substrate" (Si wafer). In the AJA tool at Cornell Nanoscale Facility (CNF), the arrangement is as shown in Figure 3 below, where the substrate is facing down and the target sputters towards it. Rotation of the substrate

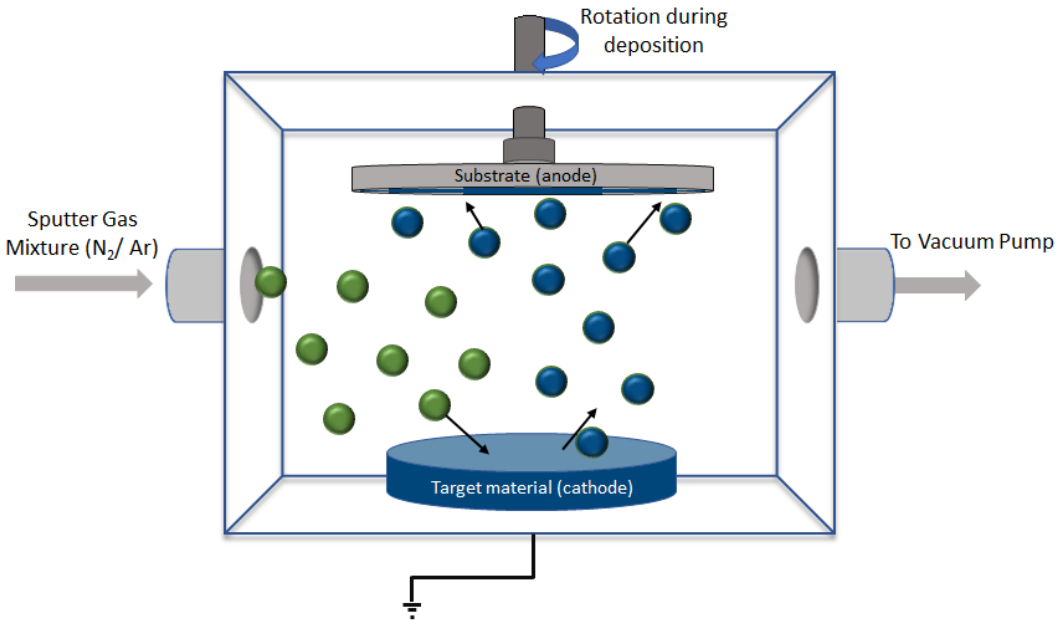

Figure 3: Sputter Deposition Mechanism

holder during deposition ensures uniform growth of film.

The sputter gases are fed into the vacuum chamber. For Ta deposition, only Ar gas ions are fed into the system whereas for TaN, N_2 gas is accompanied with it. The target material (Ta in this case), which is 3 inches in diameter and 0.25 inches thick, is the cathode. It is bombarded with the sputter gas ions. This ejects negatively charged ions from the target

which is attracted to the positively charged substrate. This is the basic mechanism for film growth during sputter deposition.

2. Specific Heat Capacity at Constant Pressure using DSC Q20

The Differential Scanning Calorimetry (DSC) Q20 is a thermal analytical technique that measures the amount of heat required to increase the temperature of a sample compared to a reference, as a function of temperature. The heat flow curve (in mW) gives the specific heat capacity, c_p, in J g^{-1} K^{-1}, from the following equation:

$$c_p = \frac{1}{m} \frac{\text{Heat Curve from DSC}}{\text{Heating Rate of Sample}} \quad (1)$$

Raw Data

pressure

Mass of Sample

The DSC is a very sensitive tool and requires very small amounts of samples for accurate measurements. The sample size is usually in mg and collected in aluminum sample pans

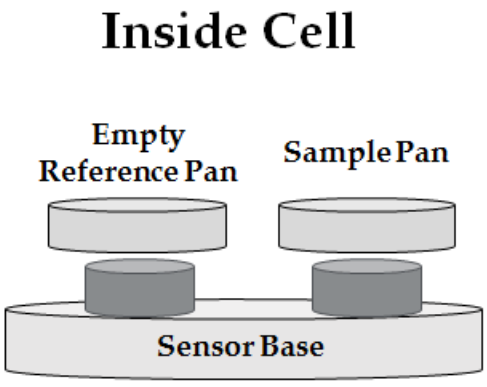

Figure 4: Cell view of the DSC Q20

that are about 5mm in diameter. These pans sit on a sensor base inside the cell of the DSC as shown in Figure 4 above. The temperature of the sample and reference pan are detected using this sensor. The amount of heat required to reach the specific temperature is the raw data and referred to as heat flow in mW.

The specific heat capacity of a substance is information on how much energy is required to raise the temperature of a unit gram of the substance by 1°C. Specific heat capacity can be at constant volume, c_v, or constant pressure. Constant pressure specific heat capacity, c_p, is easier to measure than c_v because it requires a high amount of pressure to maintain a constant volume of the sample. Maintaining a constant pressure while the sample can freely expand or contract is much more straightforward. C_p represents the thermal storage capacity of a system [20]. A substance with a lower value for specific heat capacity will require less energy to heat up than a substance with higher specific heat capacity. Thus, for TaN films on integrated circuits, a high value for specific heat capacity value at constant pressure is desirable so that the temperature of the films is not raised significantly as an effect from heating the substrate for processing or overall increase in heat flow in the system.

According to the Dulong-Petit law, the specific heat of a material enters a region of saturation above the Debye temperature, above which the value for specific heat does not change by more than 30% over the next 2000 K [8].

The Debye model estimates the phonon contribution of a solid material towards the specific heat capacity [21]. The Debye temperature of a material, θ_D, is the highest temperature that can be achieved from a single normal vibration within a crystal [22]. According to literature [8,23], the Debye temperatures of bulk Ta and TaN are 230 K and 580 K respectively. However, it has been seen in literature, that Ta does not necessarily follow the assumption

made by Dulong-Petit law [8] at elevated temperatures. This has also been observed with molybdenum, niobium and vanadium [23- 25] and attributed to electronic contributions to specific heat and thermal formation of lattice imperfections when increasing temperature [26, 27].

3. Low Temperature Resistivity Measurements of Thin films

As discussed earlier in Chapter 1, the desired resistivity of TaN films depends on the application where GMR applications require high resistivity to reduce eddy current loss and diffusion barriers would require low resistivity to prevent from a high voltage drop across the Cu interconnect layer [3,7]. It is therefore an important property to control and measure on deposited TaN films. The change in different variables such as N_2 partial pressure and temperature will not only help determine the ideal parameters for desired application, but also the stability of electrical properties with changes in temperature, which an electronic device will most likely be subjected to. Resistivity at low temperatures of conductive materials are of interest as the vibrations from a metal are reduced and should increase electron mobility, which in turn, increases conductivity.

The Physical Property Measurement System (PPMS) available at CCMR uses DC current and a 4-point probe to generate raw data on the resistivity of thin films. The equipment used was a Quantum Design PPMS which uses helium gas at low pressures (~13 Torr or 0.0013 atm) to cool the sample. It is a temperature variable measurement system where the thin film sample is wire bonded or soldered to a resistivity puck, which is a PPMS accessory, as shown in Figure 5 on the next page.

The red and blue wires shown on Figure 5 are colored for visual aid. They are ~38µm Al wires, wire bonded to the sample using a wedge bonding technique. The wires are used to

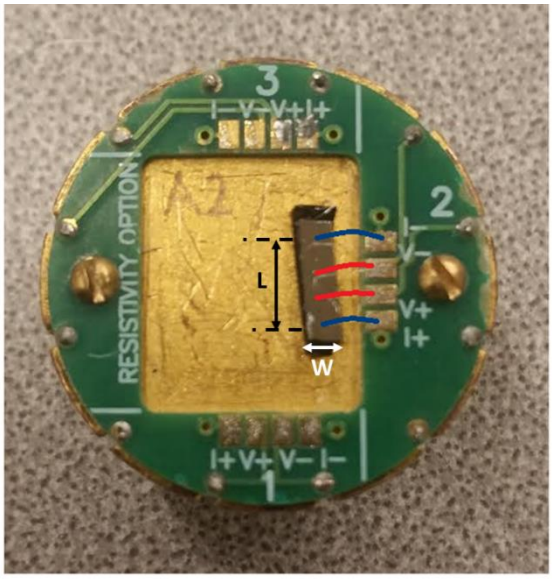

Figure 5: Thin film sample wire bonded to resistivity puck for temperature variable measurements in PPMS

connect the 4 points: I- V- V+ I+ of the resistivity puck to the thin film sample which is attached on black carbon tape. The substrate below the thin film must be insulating to ensure that the 4-point probe measurements, and current passed during these measurements, are only from the thin film sample. After wire bonding, the pucks are inserted into the PPMS which connects the electrical contacts of the puck to the rest of the system. The resistance of the sample is measured by flowing current between the outer probes, I+ and I-. Voltage V is measured between the two inner probes, V+ and V-, ideally without drawing any current between them. The resulting resistance from the sample is the raw data from the system that is plotted against temperature. The maximum temperature that the PPMS can be increased to is 400 K.

The accurate dimensions of the sample are measured using Optical Microscopic images and resistivity, ρ, is calculated using the equation below:

$$\rho = \frac{RWt}{L} \tag{2}$$

Where R is the resistance in ohms (raw data from PPMS), W is the width of the sample being tested and L is the length between the V+ and V- probes which is perpendicularly measured to W (both indicated on Figure 5). Thickness of the film is *t* in nm. The unit of ρ used in this study will be μΩ.cm. The term sheet resistance, R_S, is typically used to describe resistance in thin films with unit of Ω/sq and calculated according to equation below:

$$R_S = \frac{\rho}{t} = \frac{RW}{L} \tag{3}$$

4. Wire Bonding for PPMS Measurements

An ultrasonic wedge bonding technique was used to connect thin ~38 μm Al alloy wires to the connection pads on the PPMS puck as mentioned above. The instrument used was a

Figure 6: Variables in TPT HB05 wire bonder

manual TPT HB05 Wire Bonder available at CCMR. In this system, a wedge tool is threaded with Al wire (Figure 7 on next page) and bonds are created between wire and sample using ultrasonic power and force at ambient temperature. The wire is then extended to the connectivity pad on the PPMS puck and then cut free. The force and ultrasonic powers can be adjusted via a 4" screen on the instrument manually. The correct force and power for Ta films were found through trial and error and shown on Figure 6 on previous page. It is also important to ensure a clean dust free sample when wire bonding. The variables of the wire bonder and typical values that ensured bonding are shown in the image below.

Bond 1 is typically the thin film of interest (Ta) and Bond 2 is for the gold pads on the PPMS puck (refer to Figure 5, pg. 22). There are up to 20 program slots on the software which can be saved by different users per desired material to be bonded. US is the ultrasonic force in mW, time is in milliseconds and force is in cNm. The clamp button closes and opens the clamp on the thread. The clamp should always be closed during bonding and is open only when readjustments need to be made on the wire tail or when the wedge needs to be rethreaded with wire. The tail is the length of wire in μm at the other end of the bond and can also be readjusted. The tail and wedge arrangement for wedge bonding is shown in the simple schematic on Figure 7 below.

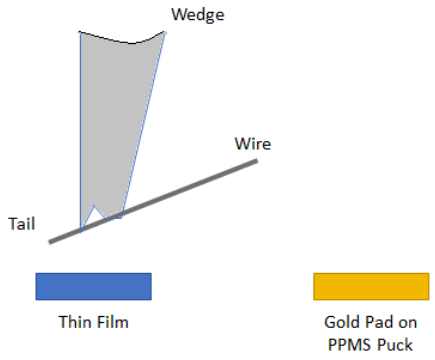

Figure 7: Side view of wedge bonding a thin film to the gold pad on PPMS puck

5. Nanoindentation for Hardness and Young's Modulus

Nanoindentation is a means by which the hardness and Young's modulus of an unknown material can be measured by indenting a small volume of the material with a very small probe of known material, most usually diamond, due to its extremely high hardness.

During indentation, the nanoindenter measures the resulting loads of the probe and displacements continually. From this load-displacement data as shown in Figure 8 below, the hardness and modulus of the sample can be calculated. The surface roughness can also be measured by profiling the surface with the mechanical probe, similar to Atomic Force Microscopy (AFM).

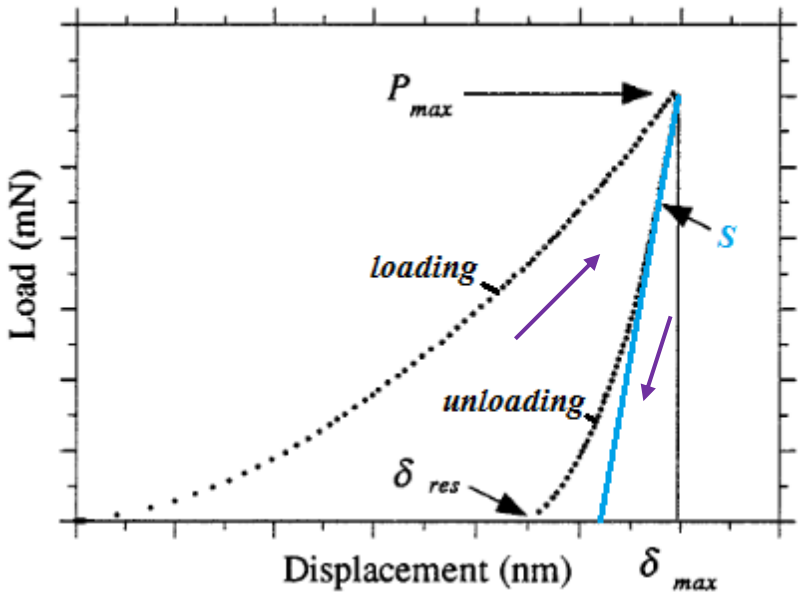

Figure 8: Typical Load-Displacement Curve from Nanoindentation Experiments [28].

The load, P, required to indent the material at a specific depth and the contact area, A_C, of the resulting indentation can be used to calculate the hardness, H, of the material by equation

provided below:

$$H = \frac{P}{A_C} \tag{4}$$

The initial slope of the unloading curve gives a contact stiffness value, S, which can be used to calculate reduced modulus, E_R, as shown in equation below [31]:

$$E_R = \frac{\sqrt{\pi}}{2}\frac{S}{\sqrt{A_C}} \tag{5}$$

The reduced modulus is related to the elastic properties of the sample and the indenter by equation 6 below [31]:

$$\frac{1}{E_R} = \frac{1 - v_i^2}{E_i} + \frac{1 - v_s^2}{E_s} \tag{6}$$

where E_i and v_i are the Young's modulus and Poisson's ratio of the indenter and E_s and v_s are the Young's modulus and Poisson's ratio of the sample, respectively. For the diamond indenter, E_i is assumed to be 1140 GPa and v_i is 0.07.

The Poisson's ratio of the sample, v_s, cannot be measured from a standard nanoindentation experiment, but a nanoindenter can be used to probe a free-standing beam created via fabrication processes. This bending experiment can be utilized along with basic beam theory to calculate the exact Poisson's ratio of the sample. For this thesis, the Poisson's ratio of Ta is assumed to be 0.34 [29] and that for TaN is assumed to be 0.25 as nitrides tend to have a

lower Poisson's ratio than the pure metal form and additionally, the Young's modulus is not effected significantly by the Poisson's ratio [30].

Nanoindentations were performed by Joseph Carloni, a PhD student in the Materials Science and Engineering department at Cornell University, who works with Professor Shefford Baker. A Hysitron "TriboIndenter" (TI-900) in Bard Hall, Cornell University is used for these measurements.

The nanoindenter probe used for measurements is a "Berkovich" shaped (see Figure 9 below) diamond probe with a ~120 nm radius at the tip. The shape of the tip is a three-sided pyramidal shape.

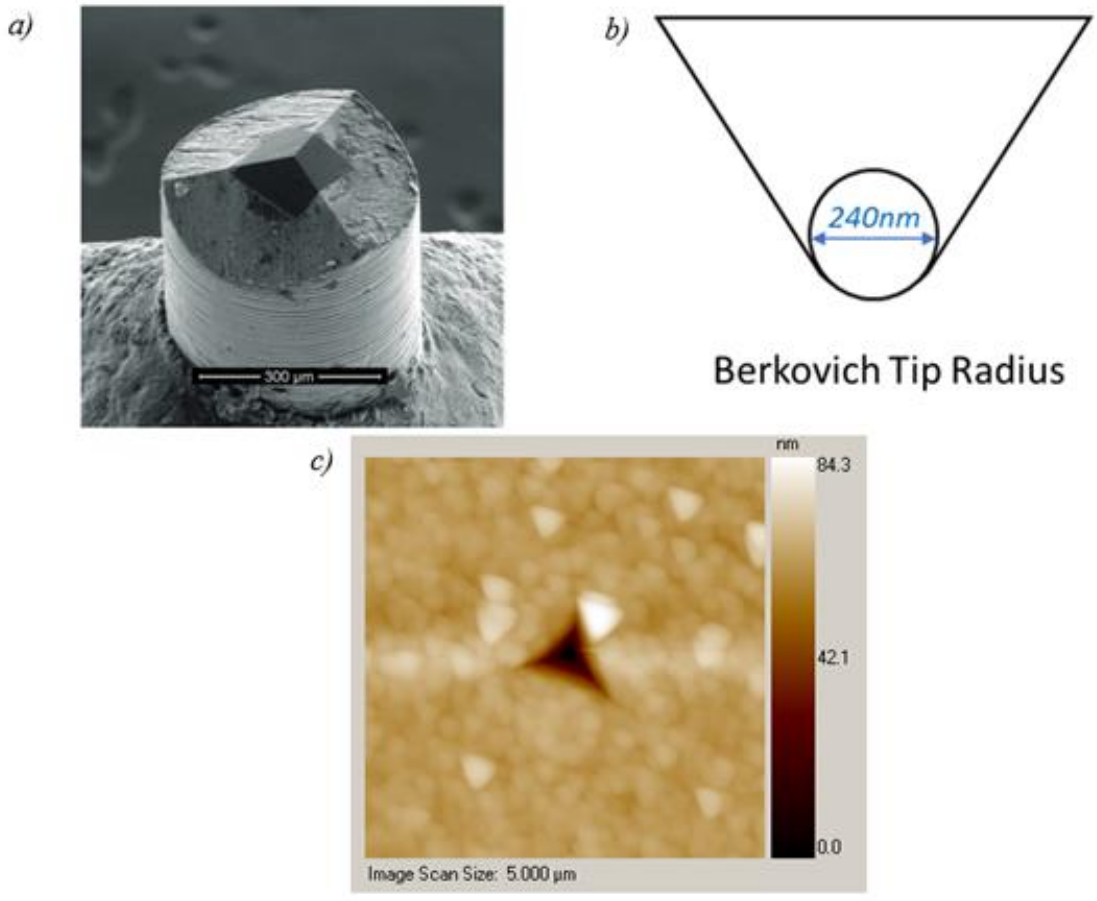

Figure 9: Berkovich tip of the nanoindenter: a) SEM image of the Berkovich tip [32]; b) the side view of a 120nm tip radius; c) typical shape of nanoindenter on sample

Ideally when an indenter is infinitely sharp, the contact area can be easily calculated. However, like all indenters, the Berkovich tip has a finite radius which may contribute to the shape of the nanoindentation to be slightly curved, which impacts calculations for hardness and Young's modulus. To account for this, an area function is calibrated for each tip using a standard fused-silica sample with known modulus. During calibration, several nanoindentations are made on the sample at different peak loads to determine the A_C and contact depth, h_C. The A_C and h_C are then plotted and fit with the following equation [31] to produce the required area function:

$$A_c = \int f(h_c) = C_0 h_c^2 + \sum_{i=1}^{i=8} C_i (h_c)^{2-i} \tag{7}$$

$C_0 h_c^2$ is equal to $24.5 h_c^2$ for an ideally sharp Berkovich nanoindenter. C_i, in the summation part of the equation, accounts for the roundness of the tip. Once the area of contact is known, the hardness can be calculated using equation 4 on page 26 [31].

The measurements are carried out at ambient temperature and pressure. Square samples of about $1 cm^2$ can be glued to the puck for measurements. Sample height must be less than 2cm. The as-deposited thin film samples are smooth enough to be measured using the nanoindenter.

The software used for the system is called *TriboScan*. For the current set-up, 10 µm square raster scans at 1 Hz and a 2.5 µN setpoint typically produce satisfactory results. The surface roughness is calculated using the *TriboView* analysis software as the root-mean squared (RMS) deviation from a plane across the entire scanned surface. Accurate measurements

cannot be made for depths less than 10 times the RMS value. Another important restriction is contact depth which cannot be less than 1/3 the tip radius.

For a 120nm radius Berkovich tip, the absolute minimum indentation depth is 40nm, and an ideal roughness (to access this minimum depth) is less than 4nm RMS. Larger indentations can be made to account for the roughness values. Finally, since the maximum load of the transducer is 10 mN, the maximum indentation depth is limited by the hardness of the sample.

To avoid substrate effects for thin film measurements, at least 10 times the minimum indentation depth of 40nm should be deposited, i.e. 400nm of film. Indentations made across a range of contact depths will ensure that substrate effects are effectively eliminated in measurements.

During measurements, the software produces raw data in the form of load-displacement curves. If the tip area function has already been accurately calibrated, the software utilizes the equations presented above and further concepts presented in literature [33] to calculate the hardness and reduced modulus of the sample material at each contact depth where an unloading occurs. The yield stress, Y, of the material can be estimated from the hardness by using equation 8 below, and the Young's modulus is related to the reduced modulus by the Poisson ratio of the sample and the elastic properties of the diamond tip as shown in equation 4, 5 and 6 presented above.

$$H = 3Y \tag{8}$$

The tangent modulus and/ or work-hardening exponent of the sample can theoretically be estimated from the amount of piled-up material surrounding an indentation, but there is currently no standard method or set-up available for doing this.

6. FleXus Stress Measurements

Thin films may induce stress on substrates and this is an important parameter since mechanical stresses on substrates for an electronic device may cause surface changes, cracking and other defects which may also lead to a decrease in conductivity and film uniformity. When a thin film is deposited on a substrate, the stress may either be tensile or compressive as shown in figure 10 below.

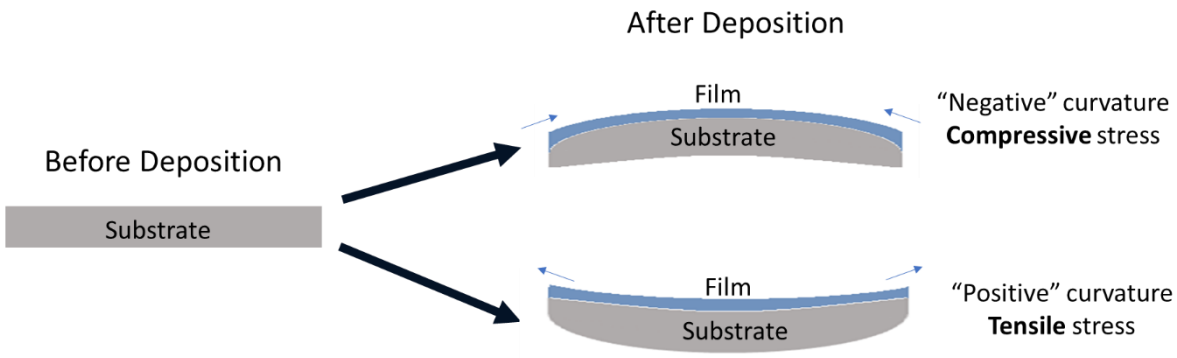

Figure 10: Schematic view of stresses induced by thin films on substrates

For integrated circuits, these values for stress should ideally be close to 0 MPa, to keep the shape of the substrate intact, and avoid inducing film defects. Stress measurements for the thin films in this thesis are measured using the Toho Flexus Film Stress Measurement System in CNF. The system assumes the substrate and film thicknesses to be uniform. As stated before, the AJA sputter deposition tool can produce films with 99% uniformity due to rotation of sample during deposition. The biaxial stress is also assumed to be uniform.

The tool uses a laser scan technique with 2 wavelengths available at 670 nm and 780 nm. Dual wavelengths may be used to maximize the reflected signal from the substrate, however, the 670 nm wavelength was sufficient for this study. The laser scans the 4" wafer

across its surface at different orientations for surface profiling. 3D plots are also available in the software which give 3D visualizations on substrate changes with film deposition.
The convention for the tool is that when the stress values are positive, it indicates a tensile stress and change in curvature is more than zero. When stress values are negative, the stress is compressive with change in curvature less than zero. The change in substrate shape from film deposition is shown in Figure 10 on previous page.

The stress induced by films on substrate is found by measuring the radius of curvature before and after film deposition. The basic principle of this equipment uses the Stoney's equation for measuring an approximate stress value for films. The Stoney's equation used by the system is shown in equation 9 below.

$$\sigma = \frac{1}{6}\frac{E_s}{(1-\nu_s)}\frac{t_s^2}{t_f}\left(\frac{1}{R}-\frac{1}{R_0}\right) \tag{9}$$

In equation above, σ is the stress, E_s is the Young's modulus of substrate, v_s is the Poisson's ratio of substrate, t_s is thickness of substrate, t_f is the thickness of film and R and R_o are the radii of curvature after and before film deposition respectively.
Biaxial modulus is the ratio of E_s to $1\text{-}v_s$.

7. General Area Detector Diffraction System (GADDS)

The Bruker D8 GADDS, available in Bard Hall at Cornell University, uses a poly-cap focusing system to focus a very intense beam from an X-ray source onto the sample. The beams can be aligned down to 0.3mm which reduces the requirement for sample size to collect data. A large sample stage with X-Y-Z controls and phi rotation can accommodate large samples as well and allows automated wafer mapping. The X-ray source has Cu and Co radiation. The instrument provides very fast data acquisition for phase identification and crystallographic texture analysis.

Below are example images obtained from GADDS and how a sample can be distinguished from being single crystal, polycrystalline, textured and amorphous.

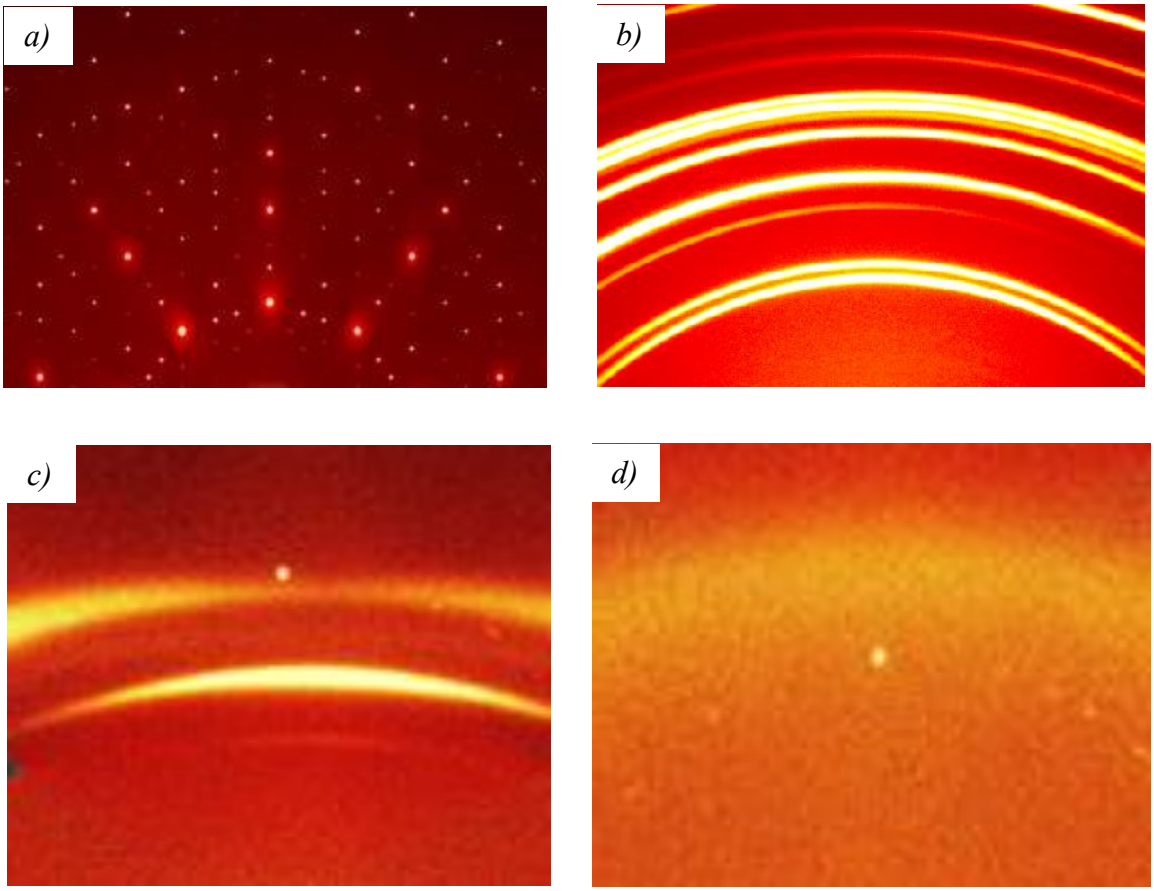

Figure 11: GADDS images of a) single crystal; b) polycrystalline sample; c) textured sample; d) amorphous sample [34].

The single crystal images have single spots whereas a polycrystalline material has several arcs of the same thickness across the arc. A textured sample has arcs of varying thicknesses whereas an amorphous material has no distinct spots or arcs. It should also be noted that, when the laser beam from GADDS is not able to focus on the sample properly, the resulting image will be similar to the amorphous image.

GADDS measurements also provide distinct peaks for samples which allow crystalline phase identification of samples as the beam incident angle, θ, is changed.

Majority of metals are either hexagonal close packed (HCP), body centered cubic (BCC) or face centered cubic (FCC) [40]. Atomic packing factor (APF) defines the fraction of volume occupied by atoms in a crystal structure. It is calculated using equation below:

$$APF = \frac{NV_P}{V_C} \tag{10}$$

Where N is the number of atoms in the unit cell, V_P is the volume of one atom, and V_C is the volume of a unit cell.

The different arrangements taken on by atomic systems are listed below with their corresponding APF:

Crystal System	APF
HCP	0.74
FCC	0.74
BCC	0.68
Simple Cubic	0.52

Table 1: APF for different crystallographic phases [36]

8. Annealing

Annealing thin films in inert gases can yield a study of defects on as-deposited films. Post-deposition annealing can lead to changes in microstructure, phases, and remove defects to enhance the properties of the thin film. Annealing may also affect surface morphology and relief strains due to lattice mismatch on as-deposited film and substrate.

Along with the purpose to study the changes mentioned above, this study includes a comparison between annealed and as-deposited thin films to study how well the TaN films may be able to prevent against diffusion in real applications, their thermal stability and changes in electrical resistivity. Ideally, an electrically stable diffusion barrier would be desirable with no significant differences in resistivity between the as-deposited and annealed thin films, unless the device requires a change in resistivity incorporated in its design.

CHAPTER 2

Experimental Procedure

Introduction to Process Variables for Study

In this study, the Nitrogen to Argon ratio during reactive sputtering of TaN films is varied. This is implemented by changing the N_2 flow measurement for each sample starting with 0 standard cubic centimeter per minute (sccm) N_2 and 22 sccm Ar for the control Ta sample. The N_2 flow measurement is then increased to 4 sccm (with 18 sccm Ar), 5 sccm (17 sccm Ar), 6 sccm (16 sccm Ar), 12 sccm N_2 (10 sccm Ar) and finally 18 sccm N_2 (with 4 sccm Ar). Note that the sum of flow measurements of N_2 and Ar gases are kept constant, that is, 22 sccm. The ratio of N_2 to Ar is simply increased which increases the N_2 content in the TaN films. The higher the ratio of N_2, the more N_2 rich the TaN films are expected to be.

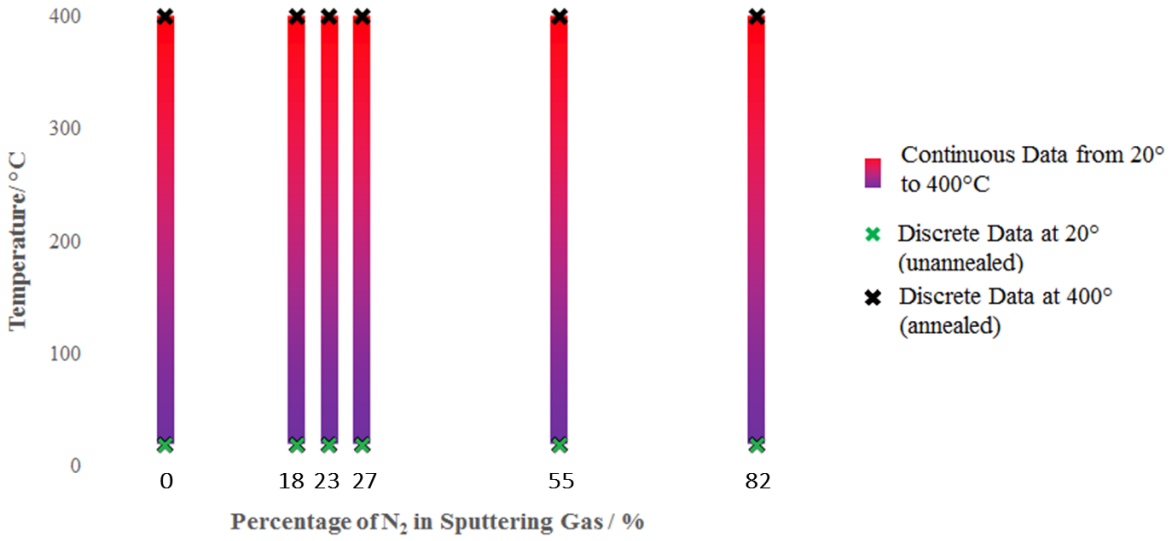

Figure 12: Process variables for study. Figure shows the continuous DSC measurements from room temperature up to 400°C and discrete data at both ends.

Detailed schematics of the process variables are shown in Figure 12 on previous page and 13 on the next page. Continuous data shown in Figure 12 is the specific heat capacities at constant pressure, c_p, of the thin film flakes, released from substrate, measured from 20° C to 400° C. The DSC Q20 equipment used, to perform these measurements, require films to be independent of their substrates which is why the flakes were released from Si. The DSC is a very sensitive equipment and minimal amounts of contamination or substrate material can effect data. This is why it is very important to ensure that film flakes are independent of their substrate and cleaned thoroughly before experiments are run.

The discrete data in Figure 12 on previous page refers to nanoindentation (mechanical properties such as hardness, Young's modulus), GADDS scans (structural properties) and AFM (surface roughness) on as-deposited and annealed thin films attached to substrates. These measurements did not require the films to be released from their substrates as the substrate effects can be effectively eliminated with such equipment.

Figure 13 on the next page shows that continuous resistivity measurements are performed starting from extremely low temperatures- from as low as 4 K (-269 °C)- up to 400 K (127 °C). These measurements were also done on films attached to an insulating layer of silicon nitride (Si_3N_4), and not directly on Si substrates.

The discrete data for films which have been annealed at 400°C in N_2 is mainly to study property changes relating to continuous data from the DSC (where the film flakes are also heated to 400°C). The continuous resistivity measurements at low temperatures is simply to study how the lattice vibrations of these expectedly conductive films reduce with temperature and should, in turn, allow more freedom in movement for the electrons,

decreasing resistivity. The temperatures for this continuous resistivity measurements could not exceed 127°C due to the limitations of the PPMS instruments available at CCMR.

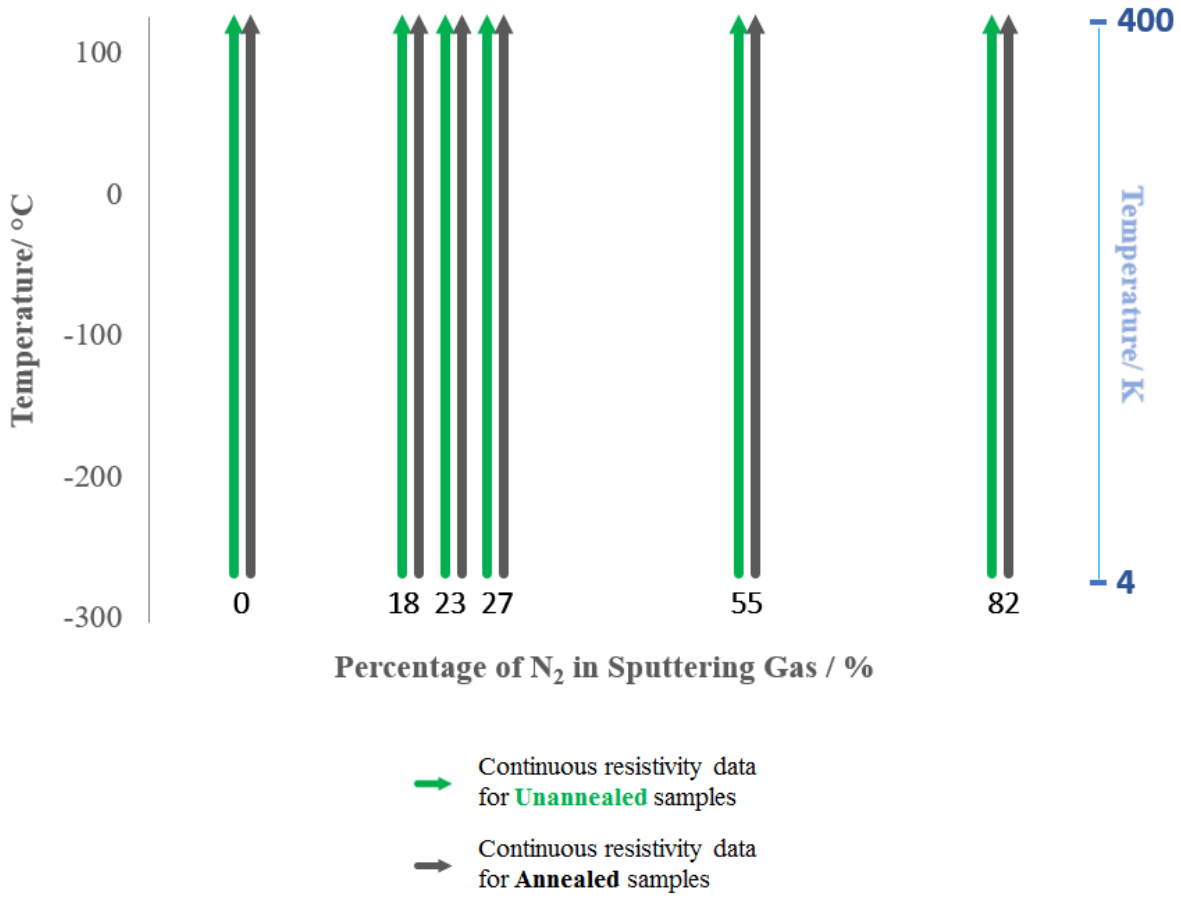

Figure 13: Process variables for study. Figure shows continuous resistivity measurements on as-deposited unannealed samples and annealed samples from 4K (-269°C) to 400K (127°C).

Sputter Deposition of Thin Films

Thin films of Ta and TaN were deposited using a PVD method of sputtering and reactive sputtering respectively. Thin films were deposited on 4" diameter Si <100> wafers of 525 μm thickness in the AJA Orion Sputter Deposition tool in CNF. The substrate used was an n-type semiconductor doped with phosphorus with an electrical resistivity of 1-100 Ω.cm. With rotation during deposition, it has been reported from the lab manual that the uniformity of films across a 4" wafer is more than 99%. Although the main purpose of this study was to analyze the effects of increasing N_2 content, a Ta control sample with no nitrogen content was also included in the experiments. The depositions are all performed in high vacuum (10^{-8} Torr).

At room temperature and at a power of 400W, the deposition rate of the Ta film turned out to be 0.25nm/s in an Ar flow of 22sccm at 7mTorr (percentage of N_2 was 0%). Two different thicknesses of 100nm and 600nm films under the same conditions were deposited.

TaN films were sputtered in the same tool under same conditions via reactive sputtering with N_2 gas. As mentioned previously, the N_2 and Ar flows were varied with each sample but the total flow of the two gases were kept constant and the percentage of N_2: Ar increases from 18%, 23%, 27%, 55% and finally to 82%. A detailed overview of the deposition conditions, including growth rate, is shown in Table 2 on next page. Table 2 also summarizes the samples and the measurements to be done on them.

Sample Number	Substrate	Thickness of Film/nm	Measurement	N_2 Flow/ sccm	Ar Flow/ sccm	N_2 Percentage / %	Deposition rate/ nm sec^{-1}
Ta	LOR 5A on Silicon	600	DSC	0	22	0	0.250
Ta_Si	Silicon	600	H, *E*, Roughness, GADDS, Ellipsometry				
Ta_SiN	Si_3N_4 on Si	100	PPMS, Stress				
TaN1	LOR 5A on Silicon	600	DSC	4	18	18	0.214
TaN1_Si	Silicon	600	H, *E*, Roughness, GADDS, Ellipsometry				
TaN1_SiN	Si_3N_4 on Si	100	PPMS, Stress				
TaN2	LOR 5A on Silicon	600	DSC	5	17	23	0.181
TaN2_Si	Silicon	600	H, *E*, Roughness, GADDS, Ellipsometry				
TaN2_SiN	Si_3N_4 on Si	100	PPMS, Stress				
TaN3	LOR 5A on Silicon	600	DSC	6	16	27	0.150
TaN3_Si	Silicon	600	H, *E*, Roughness, GADDS, Ellipsometry				
TaN3_SiN	Si_3N_4 on Si	100	PPMS, Stress				
TaN4	LOR 5A on Silicon	600	DSC	12	10	55	0.077
TaN4_Si	Silicon	600	H, *E*, Roughness, GADDS, Ellipsometry				
TaN4_SiN	Si_3N_4 on Si	100	PPMS, Stress				
TaN5	LOR 5A on Silicon	600	DSC	18	4	82	0.042
TaN5_Si	Silicon	600	H, *E*, Roughness, GADDS, Ellipsometry				
TaN5_SiN	Si_3N_4 on Si	100	PPMS, Stress				

Table 2: Summarized samples, deposition conditions and measurements to be done on each sample.
[H is Hardness, E is Young's Modulus, GADDS is for structural studies, PPMS is for Resistivity and DSC is for specific heat capacity].

Each deposition condition has 3 samples summarized in detail below and shown in Table 2 above:

1. Thick 600nm films deposited on a sacrificial layer of Lift off Resist (LOR5A), are released from Si substrate to produce film flakes which are to be examined using the

DSC measurements from room temperature (~20°C) to 400°C. The detailed steps of collecting these film flakes are shown in Figure 2 below.

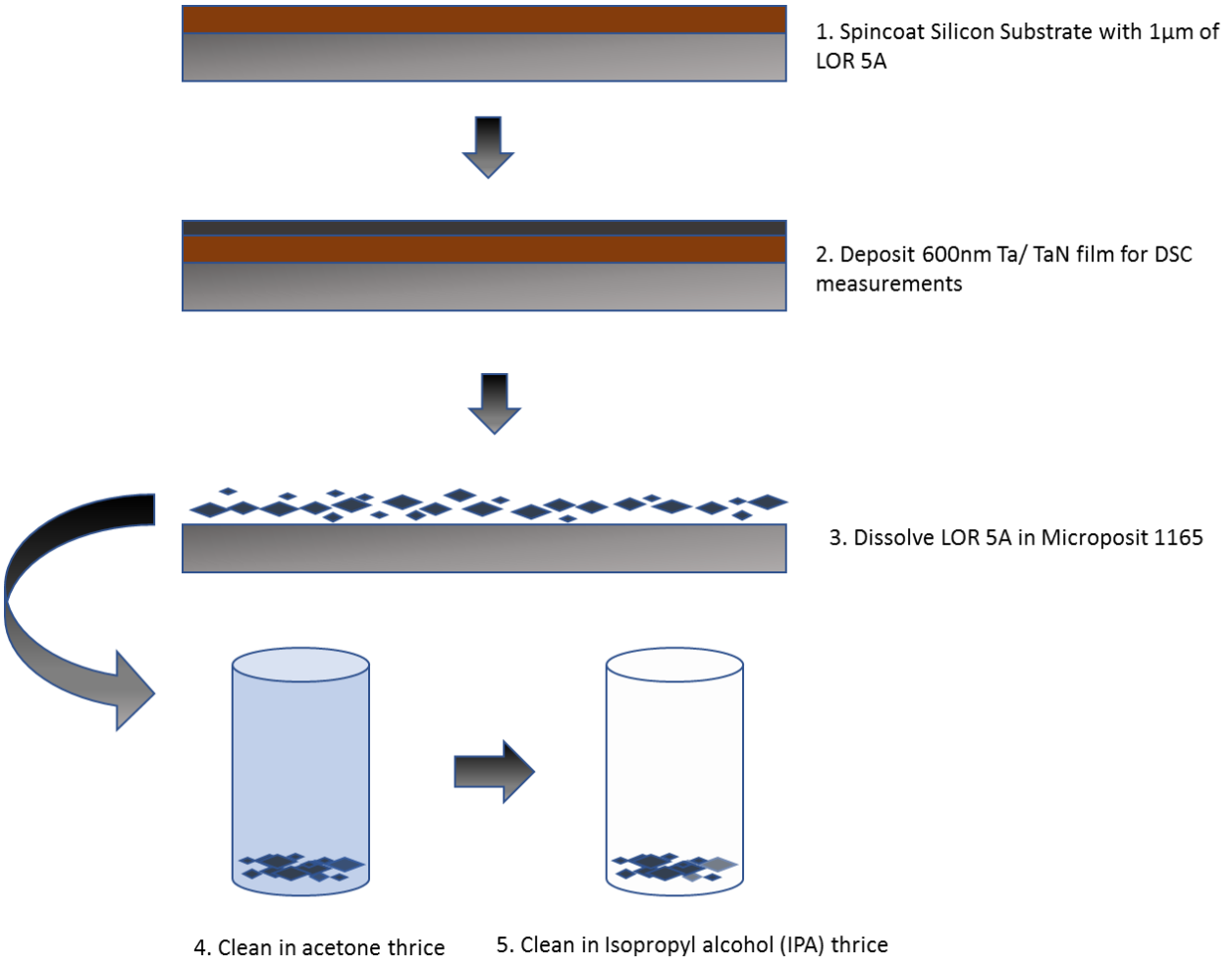

Figure 14: Collecting Ta and TaN film flakes using a sacrificial layer of LOR 5A on Si substrate. The clean steps 4 and 5 are repeated thoroughly to assure no contaminants remain.

The Si wafer is first spin coated with LOR5A at 3000 revolutions per minute (RPM) for 60 seconds on a vacuum held spin-chuck to deposit a 600nm layer of sacrificial coating. The resist is then baked at 180°C for 5 minutes to evaporate the solution and link the resist. The wafer with resist layer is then loaded onto the wafer chuck for sputter

deposition for ~600nm of Ta and TaN at 7mTorr pressure at room temperature. Note that for such processes, the temperature of deposition must never supersede 180°C to avoid hard baking of the resist. Hard baking would mean that the step of trying to strip the resist would be much more difficult and would result in the film flakes not being freed from the substrate.

After deposition, the Si wafer is soaked overnight in Microposit 1165 Remover which is a Dow Electronic Materials product used for stripping positive resists. Once the sacrificial layer is dissolved, the film flakes are released from the substrate in solution. A 2ml dropper is used to separate the flakes from the solution and transferred to a beaker of acetone to clean the organic residues that may be left from the Microposit 1165 remover and LOR5A. It is essential to clean the flakes from any residue as the DSC is a very sensitive instrument and the raw data may be compromised from such residues. DSC cell is also contaminated if measuring impure samples and should be avoided. After cleaning in acetone thrice, the process is repeated in isopropyl alcohol (IPA) three times. The film flakes are then collected onto DSC pans, a detailed description of which will be included later in chapter 3.

2. Thick 600nm samples for each N_2 flow are deposited directly on Si <100> substrates and then annealed at 400°C in N_2 gas to compare properties between the annealed and non-annealed versions. The differences in these properties are used to correlate to changes in specific heat capacity at room temperature and at 400°C from DSC scans.

3. Thin 100nm films of each film composition are deposited on thermally grown Silicon Nitride (Si_3N_4) on Si substrates to measure resistivity using PPMS measurements starting from low temperature resistivity of 4K up to 400 K.

All sputter depositions were preceded by a 5-minute chamber O_2 clean (30 sccm of O_2 flow for 5 mins at 13 mTorr). All TaN depositions were followed by a Ta target clean with no wafers in chamber by sputtering Ta on an empty wafer chuck at 3 mTorr in 30 sccm of Ar for 10 minutes. This ensures any remaining residue of N_2 content is removed from target, so that there is no effect of change in N_2 content in the following depositions of Ta or TaN.

Measuring Sputter Deposition Rate and Film Thicknesses:

Witness samples were included on the loading chuck along with all sputter depositions. The loading chucks used in the AJA Sputter Deposition tools have plenty of extra space left even after a whole 4" Si wafer is attached. The witness samples are provided by CNF to calculate the actual thicknesses and deposition rates. The witness samples are about $1cm^2$ Si chips with a patterned positive photoresist (PR S1813), exposing the bare Si substrate in some areas. After film deposition, the film deposited on top of the PR is removed by dissolving the chip in acetone in an ultrasonic beaker overnight. For thicker films the PR may be more difficult to remove. To solve this, extended ultrasonic treatment is recommended during film flake release. Also, heating on a hot plate at 100°C may create cracks within the films and PR, assisting navigation of acetone through the cracks to remove the PR and release the flakes.

After successful removal of PR, the residue pattern of the film directly in contact with the Si chip allows for step height measurements using the Tencor P10 Profilometer available in CNF. This profilometer uses a diamond stylus to measure the height differences and thus,

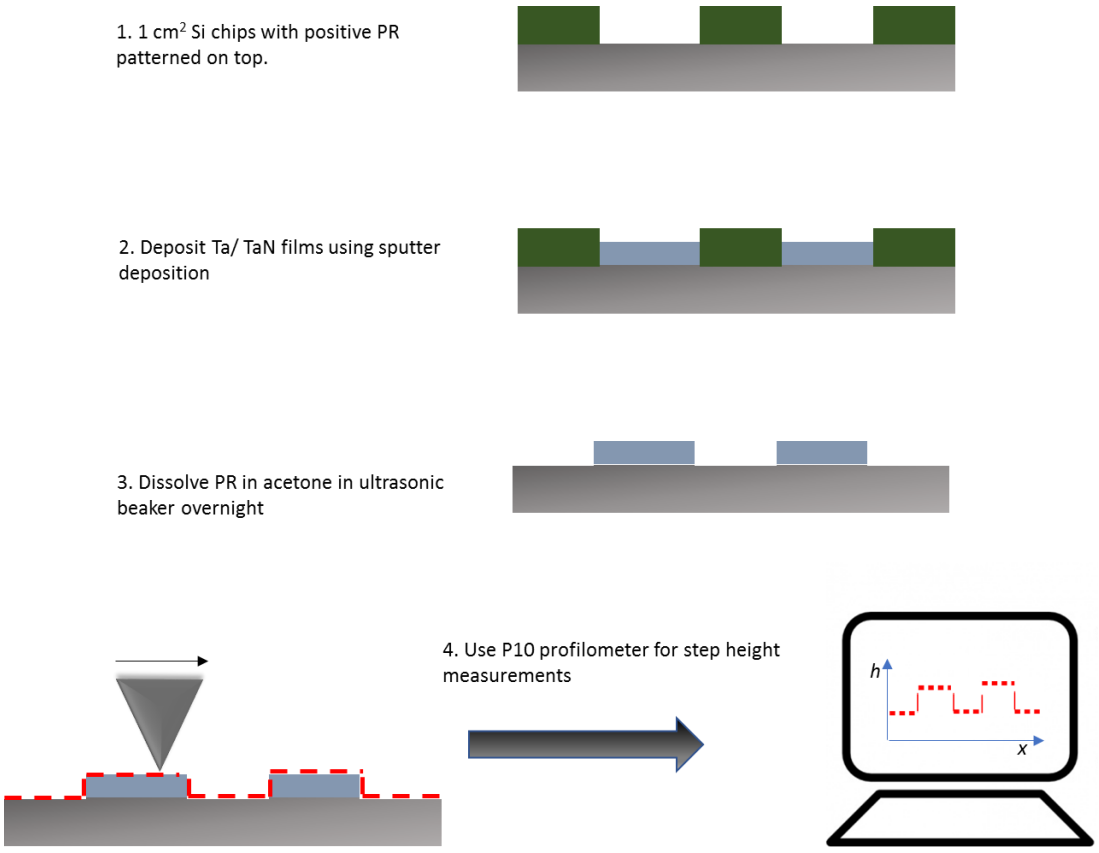

Figure 15: Using Si witness samples and P10 Profilometer to measure film thicknesses and calculate deposition rates.

reveals the actual thicknesses of the films deposited in the same loading chuck. The process of using the witness samples are summarized in Figure 15 above.

The film thicknesses are then divided by the deposition time to calculate deposition rates. Usually the deposition rates remain consistent when the target of the material in the AJA

sputter tool has not been removed or replaced. However, step height measurements were done for every sample to ensure that accurate film thicknesses are recorded for each sample.

Surface Topography (roughness) from AFM Images in Nanoindenter:

AFM in the nanoindentation tool gives a very precise study of surface topography and the images can be used to calculate surface roughness of the films down to the nanoscale. Surface roughness is a critical property for thin films especially when used in integrated circuits. As the semiconductor industry continues to scale down the dimensions of transistors, the smoothness of conducting thin films, such as TaN, effects the electrical and thermal conductivity, which in turn reduces the functionality of the whole device [37]. It has been seen that transistor noise is greatly reduced by atomically flat Si and overall performance increases [38]. This further shows that achieving sub-angstrom smoothness in films is crucial in the semiconductor industry as the transistor dimensions continue to decrease.

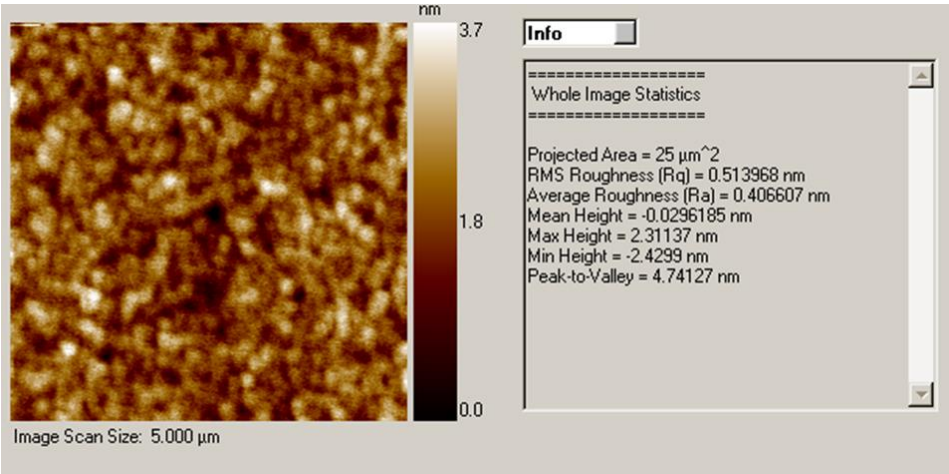

Figure 16: Screenshot of TriboView software and AFM images used from the nanoindenter

AFM imaging methods have resolution that surpasses typical stylus based profilometer and optical methods [39]. The 2 factors that affect AFM imaging resolution are instrument noise which may come from mechanical vibrations or random electrical fluctuations, and tip radius and wear of the stylus [40].

An image scan size of 5.0 μm can provide roughness values of films in RMS in Rq or average roughness in Ra as shown in screenshot of the *TriboView* Analysis software on figure 16 on the previous page.

Specific Heat Capacity Measurements:

The DSC Q20 in Bard Hall was used to make specific heat capacity measurements. Film flakes collected as shown in Figure 14 on page 40 were dissolved in IPA. 2ml droppers were used to slowly collect these film flakes at the bottom of a Tzero Aluminium pan on a hot plate at a temperature of about 60°C. This elevated temperature helps the IPA to evaporate

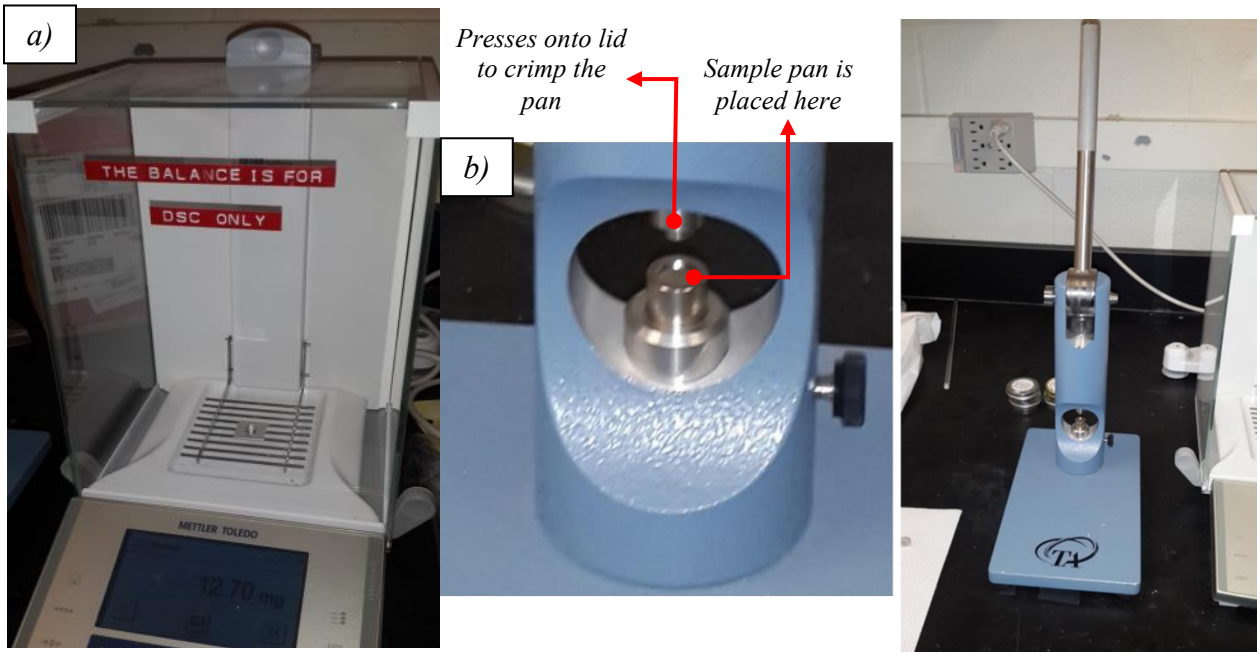

Figure 17a) Balance for DSC Pans for accurate measurements in mg; b) Crimping tool used to close the lids on the pan.

leaving a thick layer of film flakes at the bottom of the pan. When the volume of the pan has been completely exhausted, the temperature of the hot plate is set to about 150°C to completely evaporate any volatile liquid left in the pan. The mass of pan before and after the sample has been collected, is used to calculate the mass of sample. The balance used to measure these masses are a special balance dedicated only for DSC samples with a small platform in the middle of the instrument as shown in Figure 17a) on the previous page. The recommended mass for inorganics is at least 20mg and the bottom of the pan must be covered with the sample. The higher the mass, the more accurate the signal.

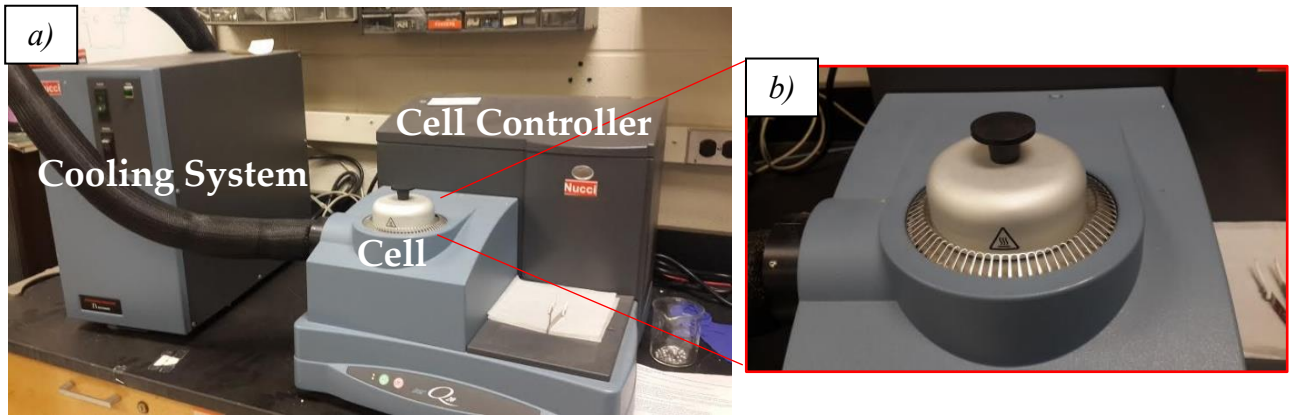

Figure 18a) Complete view of the DSCQ20; b) Zoomed in cell view.

The tool shown in 17b) on previous page shows the mechanical pressing tool which closes the lid onto the sample pan by crimping it. Both standard Al pans and Tzero Al pans have been tested and the crimping process creates dents at the bottom of the standard pans whereas the bottom of the Tzero pans remain flat and uniform. The difference between standard Al pans and Tzero pans are shown in Figure 19 on next page. Tzero Al pans also provide higher resolution, enthalpy repeatability and sensitivity, compared to standard Al pans [41].

It is very important for DSC measurements to ensure appropriate thermal contact between the cell platform and the bottom of the pan. Therefore, for DSC measurements shown in this thesis, Tzero Al pans are used.

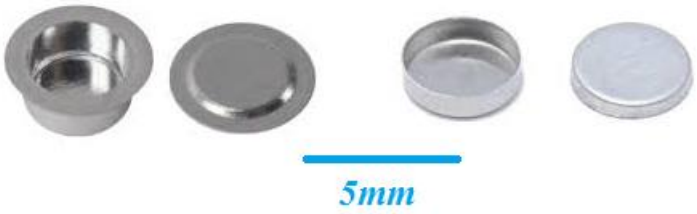

Figure 19: Tzero Al pans (left) and standard Al pans (right)

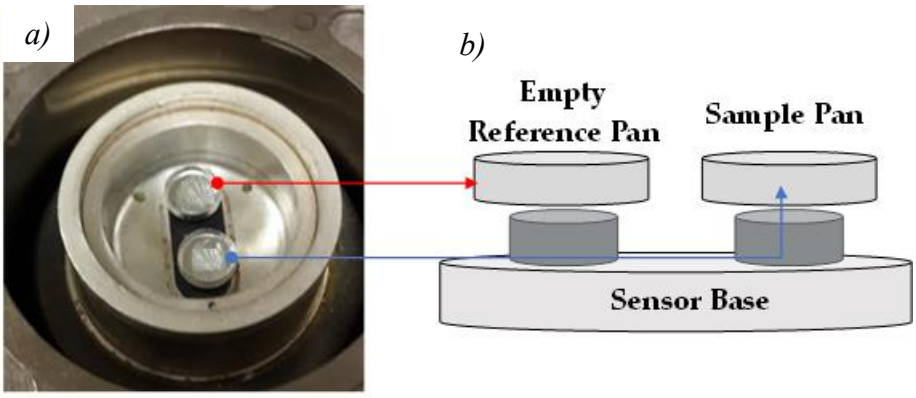

Figure 20: a) Inside the cell; b) overview of each pan

Figure 18 on previous page shows the overall setup of DSC Q20 and its components and a zoomed in view of the covered cell. The cooling system has a nitrogen gas cooling system attached, which allows the system to drop down to a temperature of -90°C. It also helps the system cool down efficiently after measurements with elevated temperatures (maximum of up to 550°C) are performed. The standby temperature of the system is 40°C. As it can be seen on figure 18a) the cell is covered to prevent significant loss of heat in the cell during experiments. Figure 20 above shows the uncovered cell and what the function of each

platform is inside the cell. The figure shows an empty pan as a reference. This empty pan should be the same type of pan used to collect the sample as the heat measurements and heat flow curve extracted from the system are essentially the difference in heat flow between the 2 pans. Therefore, for the experiments in this thesis, both the empty reference and sample pans are Tzero pans. The reference pan is always positioned towards the back of the cell and the sample pan in front.

Before any measurements are taken on the Ta and TaN samples, 3 different calibrations are performed:

1. Baseline calibration: where an empty cell without any pans is heated through the range of temperature expected in subsequent experiments. This is to eliminate any system errors in the cell. The heat flow curve produced from this calibration is used to subtract from experimental curves for heat flows in the actual samples. The baseline measurements are repeated until the baseline curve is reproducible and repeatable.

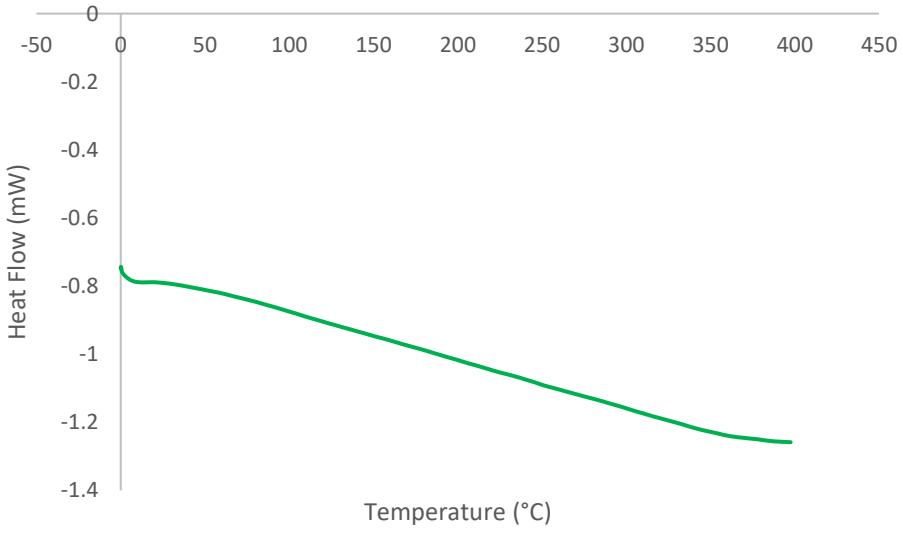

Figure 21: a) Baseline curve for empty cell heated at 10K/ min

Baselines were also repeatedly verified once several experiments were performed on samples, to ensure there was no change caused by contamination from organic residues in the samples.

As two different heating rates were used in this thesis of 1K/ min and 10K/ min,

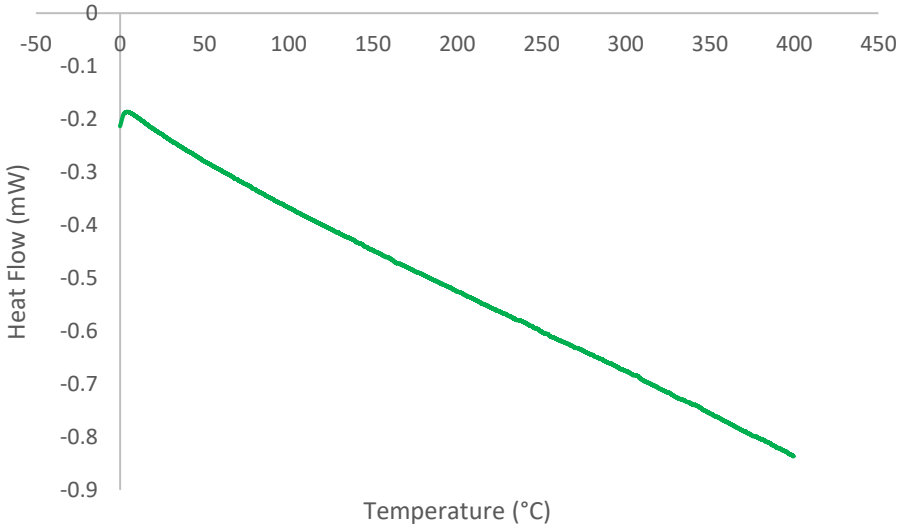

Figure 21: b) Baseline curve for empty cell heated at 1K/ min

baselines were obtained for both hearing rates. Examples of the baseline observed before experiments is shown in Figure 21 a and b above.

As shown in Figure 21, the baseline curves are different at different heating rates. Therefore, it must be used appropriately when subtracting from actual heat flow curves obtained from samples, i.e. a sample that is heated at 10K/min should be corrected with the 10K/min baseline curve.

2. Sapphire calibration, where a sapphire disc approximately 23mg is placed on the sample pan and measurements performed. The sapphire values collected are then compared with literature to calculate measurement errors. This measurement error is used to calculate

percentage errors for actual sample measurements. Figure 22 below shows the experimental and literature values.

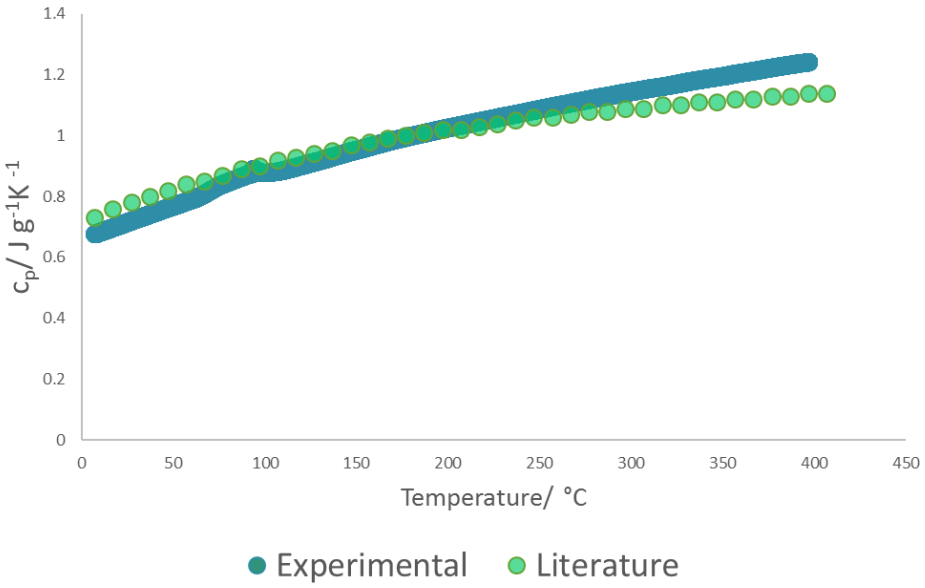

Figure 22: Specific Heat Capacity of Sapphire obtained experimentally and compared against literature

3. Indium calibration, where a small amount of indium is placed in the sample pan to calibrate for temperature in the cell. An empty reference pan is used as reference. As indium has a very low melting point of 156.6°C, it makes for an ideal material for calibrating cell temperature, without having to go to excessively high temperatures in order to see a sharp definitive peak. Indium calibrations can be down by heating the sample up to 180°C. An indication that the cell is calibrated well in temperature is, if the peak is observed at the right melting temperature of indium around 156.6 °C. Figure 23 on next page shows the cell calibration using an indium sample.

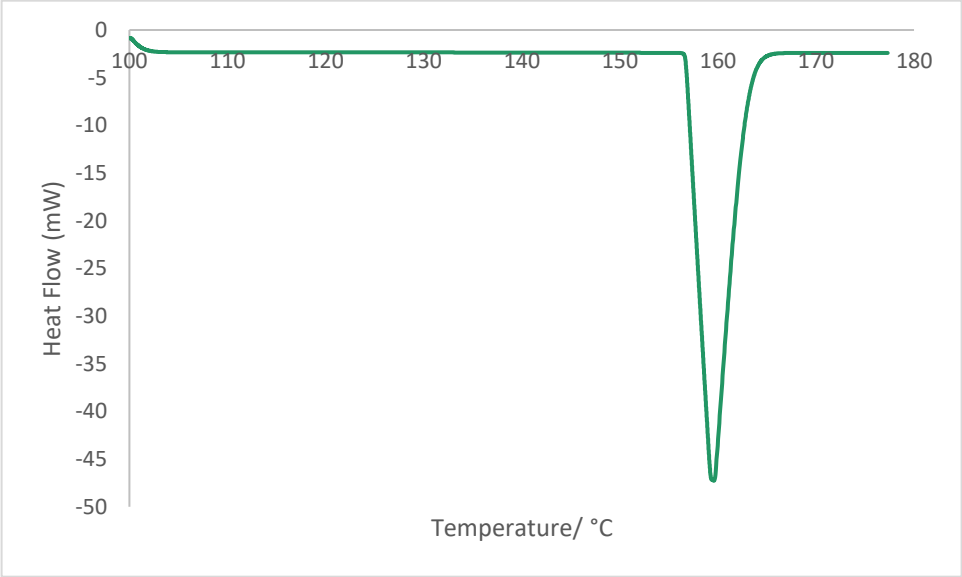

Figure 23: Indium calibration to verify the temperature response of cell

Once the calibrations are complete, the samples collected were placed appropriately in the sample pan with an empty reference pan in the back of the cell and the heat flow curves used to calculate the specific heat capacity, c_p of the sample. The p stands for pressure, as pressure is kept constant in the cell throughout these measurements. The equation 1 on page 19 is used to calculate the c_p.

Stress Measurements of thin films:

The Toho Flexus Film Stress measurement tool allows for substrates to be scanned at different orientations to calculate an average value. The typical orientations of wafer used for this study are 0°, 45° and 90° to the direction of the laser. The resulting stresses from the 3 different orientations are averaged. A ring locator is used to allocate the wafer at different orientations. The wafer positions relative to the direction of the laser and the ring

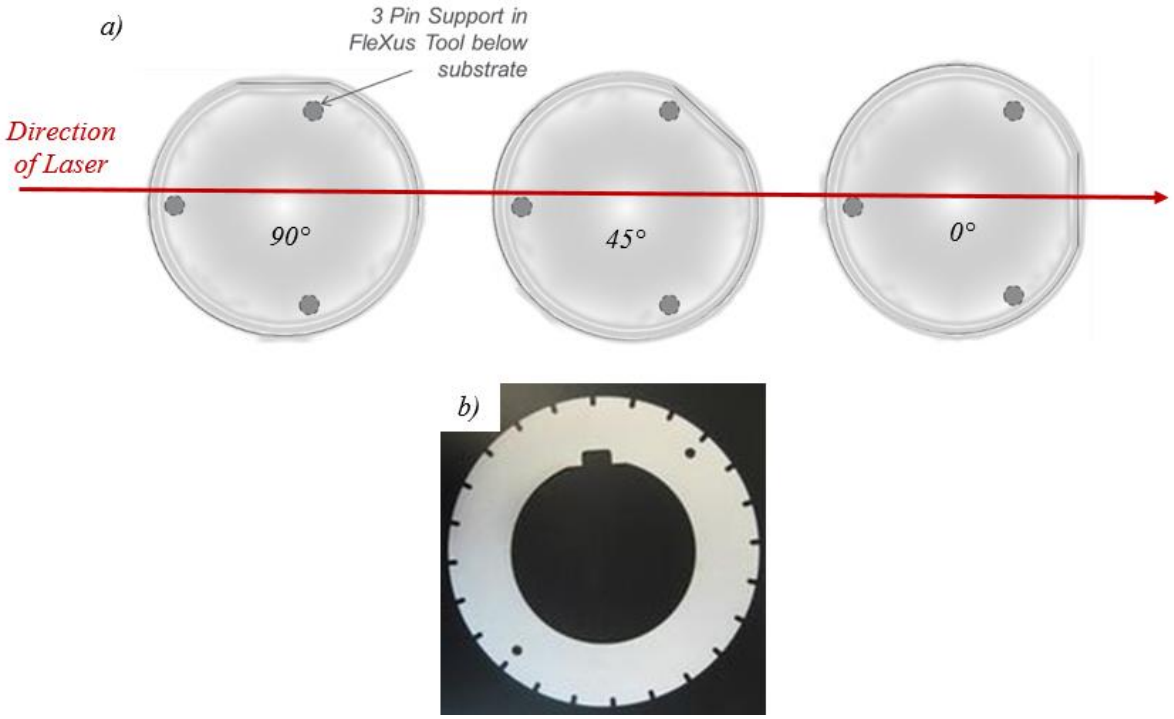

Figure 24 a) Different orientations of wafer relative to laser direction; b) ring locator to align wafers at different orientations

locator are shown on Figure 24 above. A flat head in the substrate is required for the ring locator to be used. This ring locator is made for 4" substrates specifically. However, the CNF also has a 6" substrate ring locator available.

The Si wafer sits on top of 3 support pins and should not be supported or touching the ring locator during measurements. This is to ensure that the wafer lays flat on the support pins and the ring locator does not affect the baseline of the substrate.

For <100> Si substrate the biaxial modulus in the software is 1.805 GPa, substrate thickness is 525 μm and film thickness is calculated using Profilometer method described above on Figure 15, chapter 2.

Once all the parameters are input, a 670nm laser scans across the diameter of the substrate and measures the R_O, which is radius before deposition. The process is repeated after changing the orientation of the wafer using the ring locator. Once a film has been deposited, the laser scans the profile of the substrate again to record a new radius, R. The difference in R pre-and post-deposition yields stress values in MPa using the Stoney's equation 9 as discussed in chapter 1, page 31.

Phase Identification using GADDS

The way atoms are arranged in a crystal affect the properties of the material. It has been observed that resistivity increases when body-centered cubic content in Ta increases [42]. It has also been observed that tetragonal Ta_4N_5 and tetragonal Ta_3N_4 are thermodynamically more stable, in contrast to TaN which has anti-site defects [3]. Additionally, changing the back pressure of N_2 flow during deposition leads to distinct phases such as cubic TaN, amorphous TaN and tetragonal TaN [43].

GADDS measurements were performed on as-deposited and annealed Ta and TaN films of all Ar: N_2 ratios.

Measurements were made on a range of 15°< 2θ < 60° with Cu radiation of λ= 1.54. A nickel filter was used to eliminate k-beta radiation. A cobalt (Co) radiation of λ= 1.78 is also available with an iron (Fe) filter and is ideal for Co-bearing materials.

The detector is a 2D Vantec detector, which has been calibrated during installation. At a default distance of 200 mm from the sample, the detector collects a range of ~30° in 2θ [44]. Once the raw data and images are collected, they are analyzed using the JADE data analysis software. The software includes a vast library of peaks and corresponding phases which help in identifying the crystallographic phases of the samples.

Annealing

The Ta and TaN film samples were annealed in the General Material Anneal (A1) furnace available in CNF. The annealing was performed under atmospheric pressure in inert N_2 gas

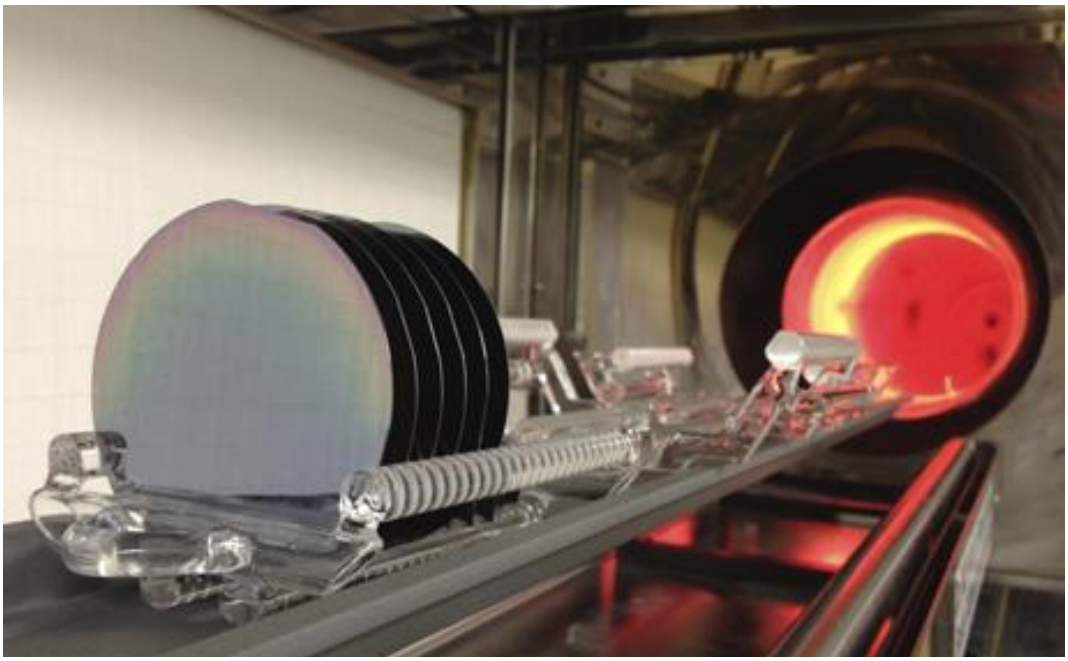

Figure 25: General annealing furnace available in CNF [44]

atmosphere and at 400° C for 30 minutes. This furnace allows whole 4" wafers and several platforms to place chips and segments of whole wafers.

Figure 25 on previous page shows the furnace in CNF and 4" wafer holders. After loading, the wafers slide towards the orange glow and the cover at the other end protects the samples from the external environment during processing. The furnace can accommodate more than 100 wafers at once. 6" substrate holders are also available. The maximum temperature of this furnace is 1100° C. The semiconductor application of interest is typically subjected to 400° C which is how the annealing temperature was chosen. Additionally, the system is capable of dry oxidation with and without HCl and H_2/ N_2 mixture treatment.

Low Temperature Resistivity using PPMS

100nm of Ta and TaN thin films of different N_2 flow were deposited on an insulating Si_3N_4 layer on Si substrate. The films were then cut into small rectangles that may fit the PPMS puck with dimension of 11.6mm into 13.6mm. The thin film samples were then bonded to the gold pads on the puck using the TPT HB05 wire bonder available in CCMR as well. The TaN films were soldered to the puck as the wire bonding parameters required extensive experimental trials. Once the PPMS puck with samples are loaded into the instrument, the maximum current (μA), power limit (μW) and voltage limit (mV) are chosen. The limits are 0.005-5000 μA, 0.001-1000 μW and 0.1-95mV respectively. The drive mode is chosen to be direct current (DC) and the limits are chosen to be 1 μA, 1000 μW and 95 mV respectively.

The temperature range for measurements are from 4 K (-269 °C) to 400 K (127 °C). The scan temperature from 4 K to 15 K is kept at 0.5 K/min for accurate temperature response

of the sample. From 15 K to 400 K, a scan rate of 6 K/min is used. 3 samples can be measured at once and a scan with such a sequence may take approximately 3 hours.

CHAPTER 3

Results and Discussion

Mechanical Properties (E and H)

As discussed earlier when introducing the properties of Ta and TaN thin films in chapter 1, the hardness of such films range between 10-18 GPa depending on the nitrogen content in the films. There is no clear trend in the mechanical properties as the N_2:Ar ratio is increased and is a result of complex changes in structures [16]. However, it has been repeatedly seen in literature that the increased N_2 content gives rise to increased hardness up to about 50% of N_2: Ar. As the N_2 flow is increased further, the hardness starts to decrease [17].

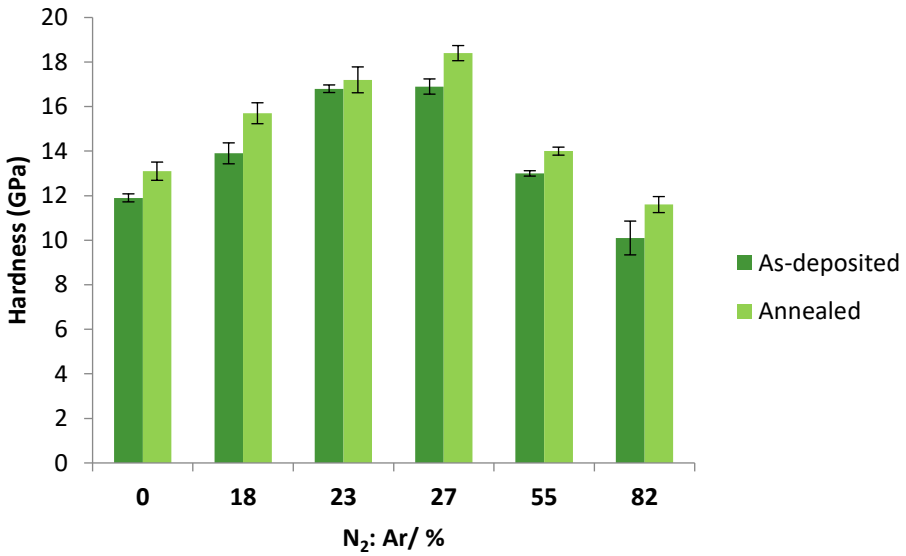

Figure 26: Hardness (GPa) of as-deposited and annealed samples of different N_2: Ar ratio

Vacuum annealing TaN films has also shown increased hardness apparently due to an effect from enhanced film density [14]. The Young's modulus (E) of TaN films ranges from 150-250 GPa [15]. Vacuum annealing has also shown to increase the E of these thin films, attributing this behavior to a decrease in defect concentration [14].

The results were consistent with literature review as shown in graphs in figure 26 on previous page. It can be seen that the hardness increases with annealing.

Figure 27 below shows the Young's modulus in GPa of deposited and annealed films. Also, consistent with literature, the Young's modulus increases for films up to 33% N_2 (6 sccm N_2 flow) and then drops. This can be attributed to the phase changes as N_2 flow is increased and will be discussed further in the GADDS result section later. In summary, the 55% N_2 flow is found to be amorphous and the 82% N_2 flow, a mixed phase of hexagonal Ta_2N and Ta_3N_5. The change in interatomic bonds and atomic microstructure may be a result of this.

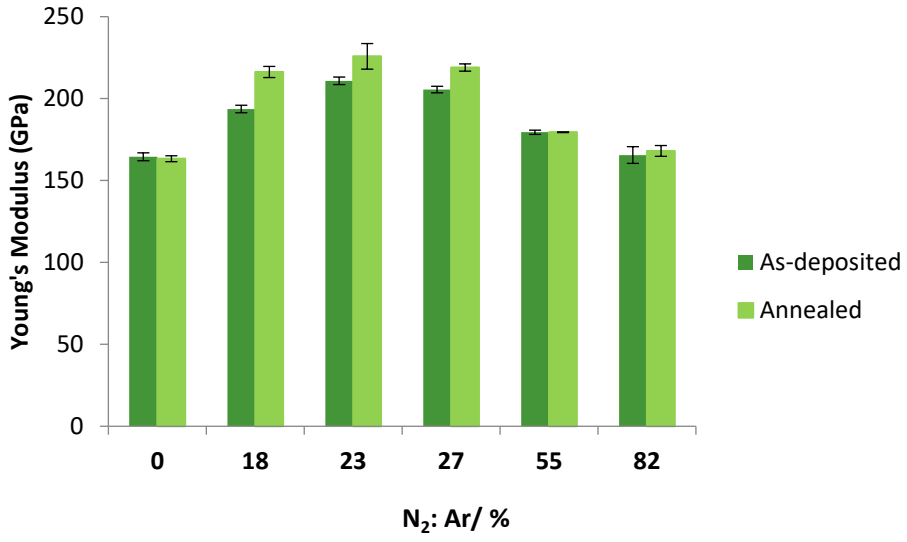

Figure 27: Young's Modulus (GPa) of as-deposited and annealed samples of different N_2: Ar ratio

Annealing treatment has also shown to increase the Young's modulus, consistent with literature. As will be seen with resistivity measurements, there is an evident change in material with annealing.

Roughness values from AFM images

Roughness of the 600nm films on Si were measured using AFM images from the nanoindenter for a scan size of 5µm. The roughness values for are summarized in the Table 3 below. There is no trend in these values and annealing does not induce much change other than for the 82% N_2: Ar sample.

Sample ID	N_2/ Ar (%)	Roughness, Ra (nm)
Ta_Si	0	0.45
Ta A	0	0.40
TaN1_Si	18	1.22
TaN 1A	18	1.35
TaN2_Si	23	0.75
TaN 2A	23	0.74
TaN3_Si	27	0.62
TaN 3A	27	0.65
TaN4_Si	55	0.27
TaN 4A	55	0.25
TaN5_Si	82	1.98
TaN 5A	82	2.30

Table 3: Roughness values for600 nm films on Si. 'A' stands for annealed films.

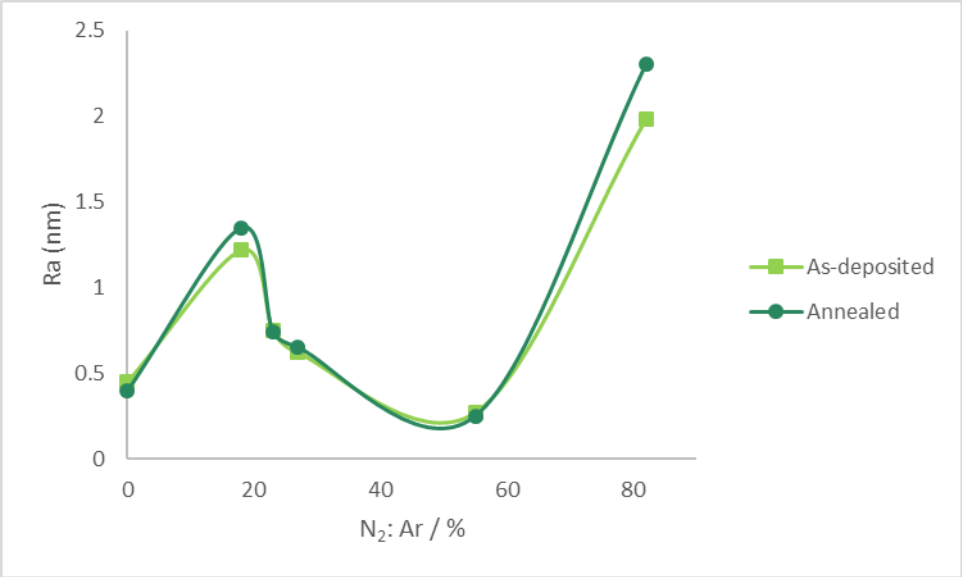

Figure 28: Roughness values for as-deposited and annealed films for different N_2: Ar ratios

As seen above in Figure 28, there is no clear trend in the roughness values for the Ta and TaN films and no significant changes with annealing. Similar lack of trend has been observed in literature. The films in this study are also smoother than what has been observed in literature, which was in the range of 1 nm [16].

Optical Microscopic Images of DSC Film Flakes

Optical Microscopic images were taken of the film flakes collected for DSC measurements. Film flakes were collected on glass slides for these images and had some liquid (IPA) residue as observed in images below. Some depositions created flakes with hollow rod like structures or flakes with some curvature as shown in Figure 29 on the next page. This limited the amount of material collected in the Tzero Al DSC pans to about 10mg for some samples. A high-volume DSC pan would be recommended for future experiments where the user is

able to collect the minimum requirement of 20mg for DSC thermal measurements on inorganic samples.

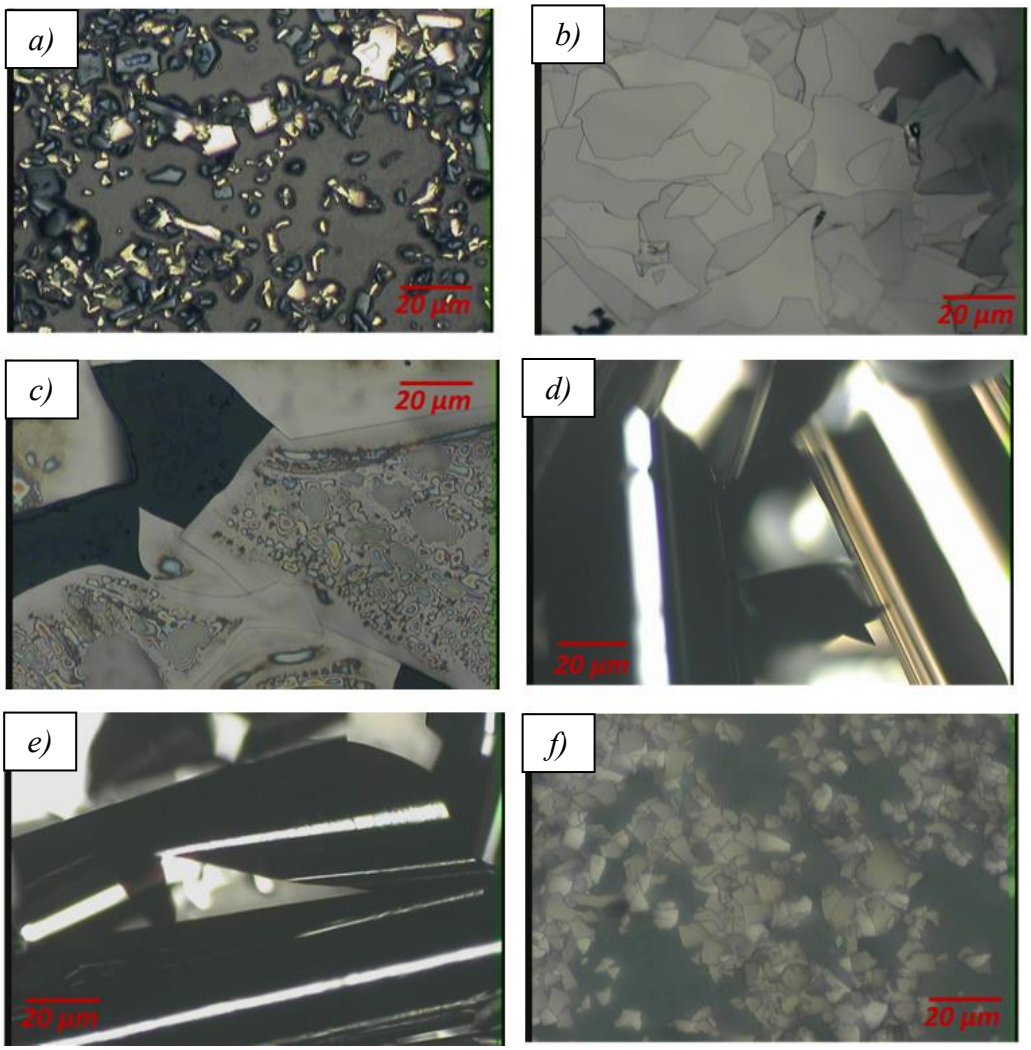

Figure 29 a) Small film flakes for Ta; relatively large film flakes for b) 18 % N_2: Ar and c) 23% N_2: Ar; rod-like hollow flakes observed with d) 27% N_2: Ar and e) 55% N_2: Ar; f) small flakes observed with 82% N_2: Ar

retain their shapes as shown in Figure 29 above. While this ensures further and thorough cleaning of the flakes from organic residues, further cleaning and collection of flakes into DSC pans becomes more difficult and arduous.

Specific Heat Capacity Measurements on Film Flakes

Specific heat capacity measurements were done on all samples, focusing the most on the 18% N_2 and 23% N_2 samples. Additionally, 99.5% metals basis TaN powder was purchased from American Elements (Product Code: TA-N-025M-P) for bulk TaN. Bulk 99.9% purity Ta sheet from Goodfellow of about 0.02mm thickness and 25mm x 25mm was purchased.

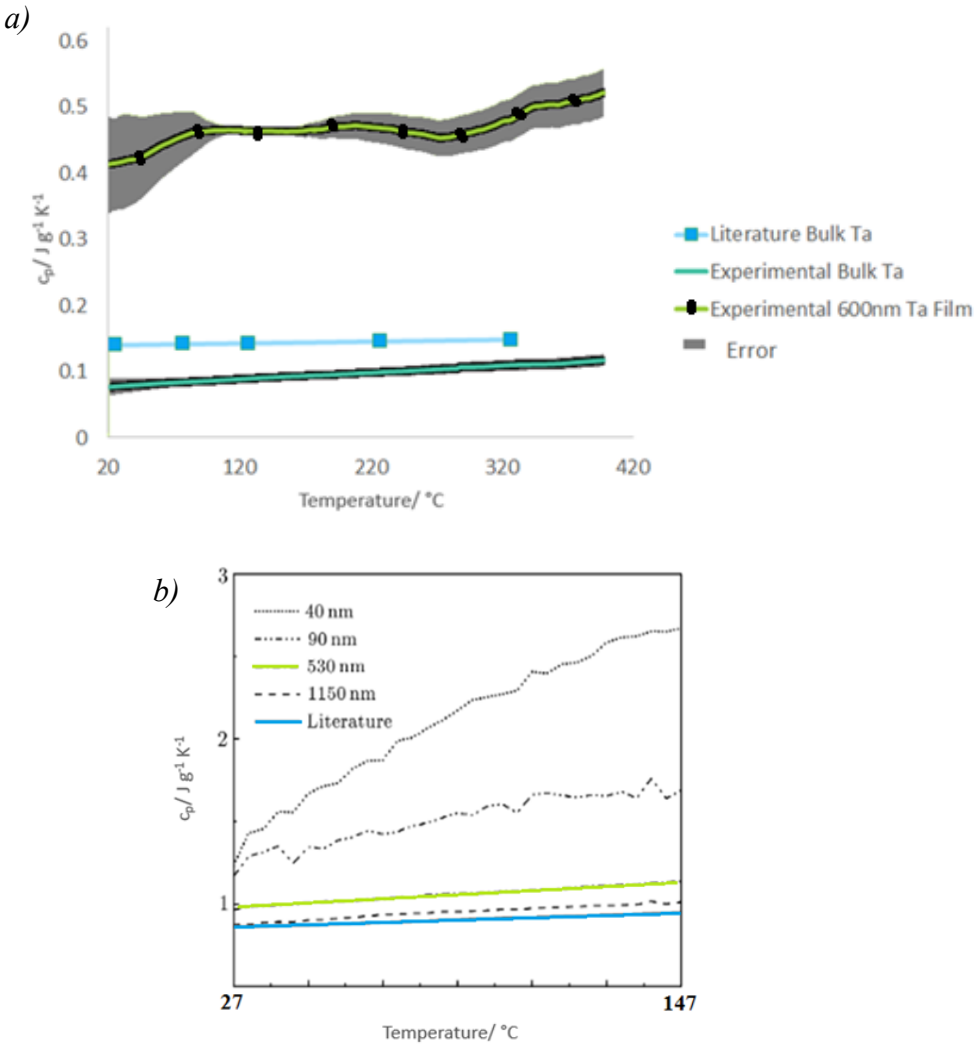

Figure 30: Specific Heat Capacity for a) Ta films compared to bulk and literature bulk values; b) Al thin films compared to bulk literature values [10]

The bulk samples were used to compare with the thin film values collected to correlate to differences seen in literature between bulk and thin film specific heat capacities

of metals. The measurements for bulk materials were done over the same temperature range from room temperature (~20°C) to 400°C. The graphs on Figure 30 on previous page show the results.

It can be seen from figure 30 that the c_p of all samples tend to increase with increasing temperature. The thin films also have increased specific heat capacity compared to their bulk form, as seen in literature. For thin Al films, the c_p becomes enhanced increasingly with decreased thickness [10]. The literature graph is shown in Figure 30b. The curve for the thin film is also consistent with literature, where slight increases in temperature lead to a relatively noticeable increase in c_p, whereas the bulk values increase at a much slower rate i.e. exhibit a curve with lower gradient. The difference in Ta measured bulk values and literature bulk values can be attributed to system errors and the nature of the sample may be different. Measurements were performed on bulk Tantalum sheets about 0.02mm thick whereas the bulk material type in literature is not specified. No additional studies have been done on the purchased bulk Ta to verify other properties and phases of the material and leads to scope for future studies. Furthermore, the crimping of the Ta sheet and ensuring appropriate contact between the bottom of the pan and the sample was not straightforward due to the shape of the sample being curvy.

Some measurement errors of the Ta films could be due to sample sizes being less than recommended value of 20mg due to the Tzero pans not being able to accommodate enough material. Most film flakes, not just limited to this deposition condition, were very thin flakes with curvatures or rod like structures as can be seen from the optical microscopy images in

figure 29, preventing from the samples that were collected to be densely packed at the bottom of the pan. Figure 31 below will clarify the issue raised.

Figure 31: Left image shows an ideal situation where a material can be densely packed in the pan to accommodate maximum amount of material. Images on right show samples collected for this study with a lot of space in between.

After enclosing the pan with a lid, the crimp press pushes the samples and closely packs them at the bottom, ensuring sufficient contact of samples with the bottom of the pan. However, the behavior and shapes of the flakes restricted the amount that could be collected. This issue can be resolved in future experiments by using a high-volume DSC pan available for purchase from TA Instruments.

Limited research exists on specific heat capacity of thin films of Ta. Additionally, there is also a need for bulk TaN values with varying temperature. Only one c_p value

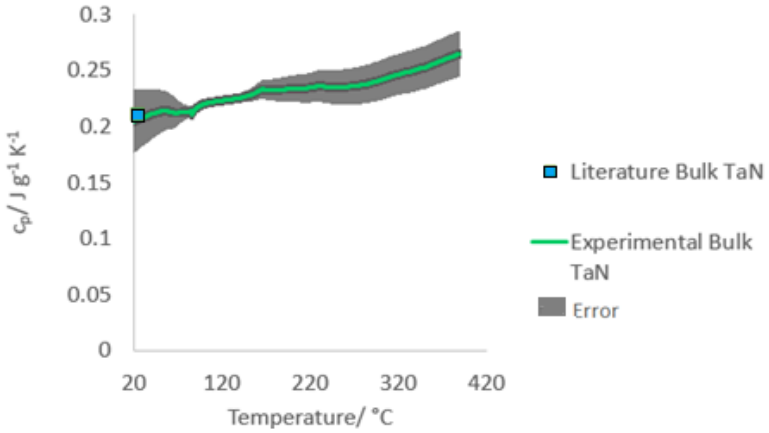

Figure 32: Specific heat capacity for TaN bulk compared to room temperature literature value [13]

was found for room temperature bulk TaN in literature and included in Figure 32 on previous page along with measured experimental bulk TaN data. The bulk value at room temperature for literature and experimental coincide, verifying, not only that the DSC is accurate, but also that the TaN purchased is like cubic TaN reported in literature [13].

Figure 33 below shows the specific heat capacities of different N_2 flow heated from room temperature (~20° C) to about 400° C.

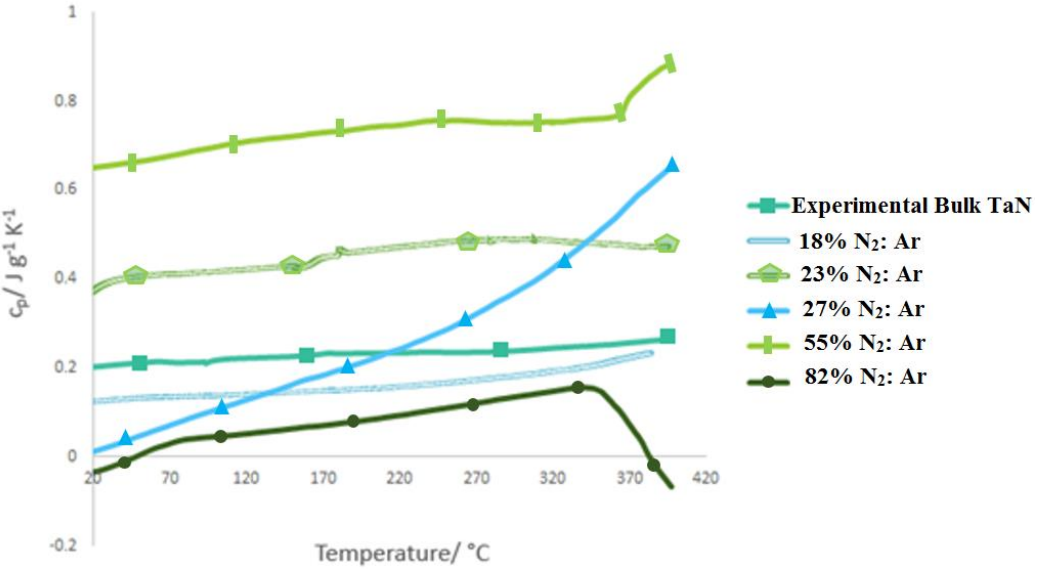

Figure 33: Specific heat capacity for TaN films compared to experimental TaN bulk

C_p for all TaN thin films increase with temperature as expected. Surprisingly, the behavior of 600nm thin films for 18% N_2: Ar and 82% N_2: Ar are lower than bulk, although the behavior of the 18% N_2: Ar curve is quite similar to bulk in terms of increase per unit temperature. This agrees with 550nm thin films of Al (Figure 30b, pg. 61), where, as the thickness of the thin film increases, it approaches the bulk curve. The 23% N_2: Ar curve has

a similar gradient to the bulk and 18% N_2: Ar curve but has enhanced specific heat capacity values. The 27% N_2: Ar curve, however, exhibited a different behavior to the rest of the samples. This could be due to the nature of the flakes, where the specific heat capacity at room temperature is shown to be lower than the actual material value. As the temperature is increased, the hollow rod-like flakes may be more condensed at the bottom of the pan, which in turn, increases the c_p. Reheating the same sample several times may verify this hypothesis.

The 82% N_2: Ar curve was repeated thrice to see the same decline in specific heat capacity around 340 °C to 360 °C. Thus, if there is a change in microstructure in this sample, it is reversible. This sample also exhibits the lowest values for specific heat capacity, and may not be desirable for applications where electronic devices require higher c_p and more resistance to heating up from increase in temperature from external factors in the device. The heat flow in these curves represents a difference in heat flow between reference pan and sample pan. A baseline curve, as shown previously, and obtained during calibration, is subtracted from the sample curve. These may introduce some errors and causes the c_p to be negative when it is theoretically not possible for a substance to cool down when the temperature is increased.

All the experimental curves mentioned thus far for specific heat capacity have been heated at a rate of 10K/ min. As mentioned in earlier chapters, a heating rate of 1K/min is also used to observe the behavior in samples and to attempt to study the activation energy if any

significant phase changes occur. 2 examples are shown below.

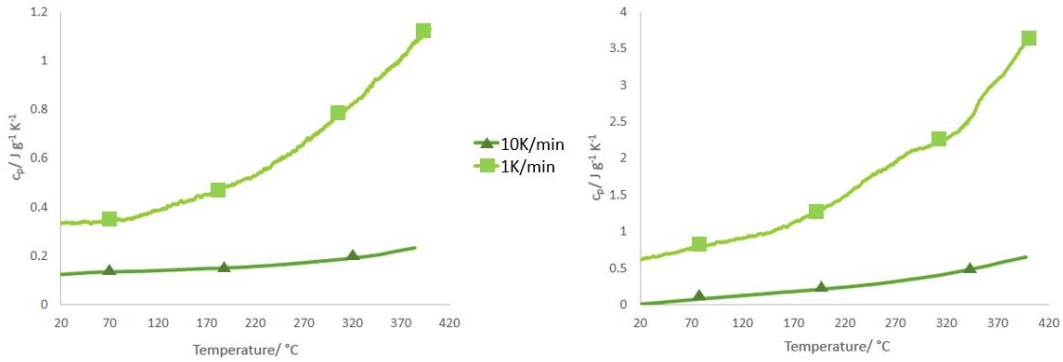

18% N_2: Ar

27% N_2: Ar

Figure 34: Specific Heat Capacity for films at heating rate of 1K/min and 10K/min

The curves are significantly shifted but not parallel to the curves of 10K/min. The enhanced specific heat capacity at lower rates may be due to the additional time that the sample is allowed to heat up. The lower heating rate is also a better measure of actual system temperature than the higher heating rate. The main purpose of reducing the heating rate, however, was to obtain an estimation of activation energy. Due to lack of a phase transition or sharp peak, this may not be obtained with current samples.

The 1K/min scans run for approximately 7 hours in atmospheric pressure without any inert gas flow. This was due to the limitations of the Q20 instrument available in Bard Hall. To verify that the sample does not oxidize, similar scans were made on same sample following the 1K/ min scans to determine repeatability. Additionally, a sample has been tested by making an intentional insertion on the lid to assess whether oxidation may occur from dents created while crimping the pan. The sample was then heated in the DSC. Results showed

that no significant changes take place in c_p although it does not eliminate the probability of oxidation of the sample as it will be observed with other measurements.

PPMS Low Temperature Resistivity

As mentioned earlier, the resistivity of TaN films have been observed to change with deposition and annealing conditions.

It has been seen in literature that the resistivity of Ta and TaN thin films fall in the range of 10^{-4} μΩ.cm, which falls in the range of a semiconductor material. The resistivity of TaN films has been seen to increase with increased Nitrogen content in several literatures [12, 13, 14]. The temperature dependence of amorphous β-phase Ta films has been seen to decrease with increasing temperature in various literature [15-16]. Furthermore, annealing Ta film is shown to decrease the resistivity of a film, which may be attributed to defect healing [16]. The graph below in 35 a) from literature shows how vacuum annealing reduces resistivity for α-β mixed phase Ta films. Figure 35 b) shows the increase in resistivity of amorphous Ta films as the temperature is decreased.

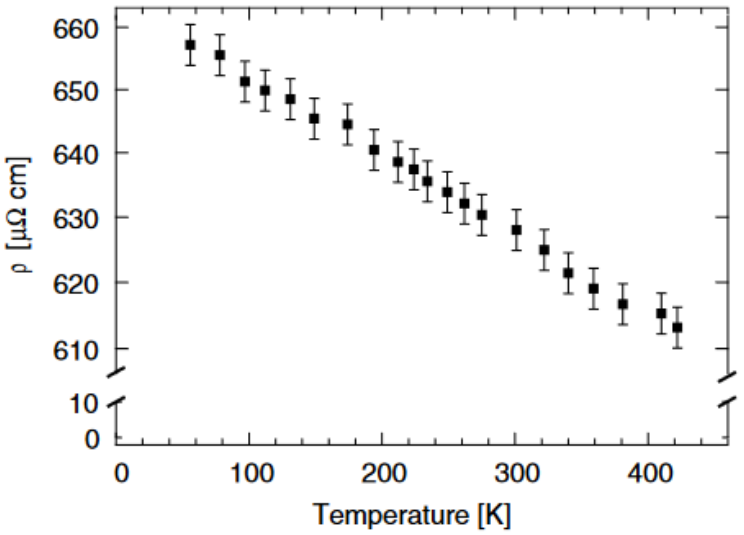

Figure 35 a) Temperature Dependence of a 40nm Ta film (e-beam evaporation) [16]

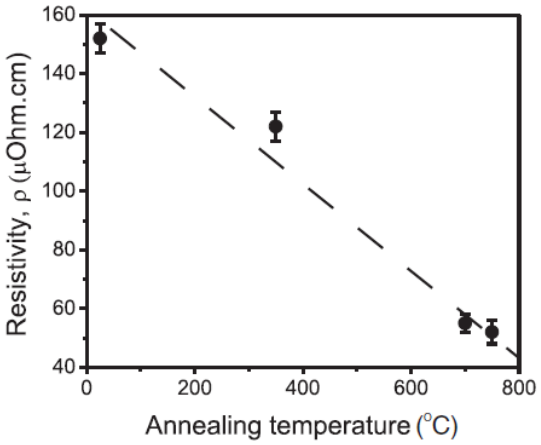

Figure 35 b) Vacuum annealing reduces resistivity of Ta films (α-β) [47]

As shown in figure 35 below, the experimental data for Ta films is consistent with literature, where the resistivity increases with decreasing temperature. Although it is expected for lattice vibrations to reduce with lower temperature and increase electron mobility, thus decreasing resistivity, it has not been explained in literature as to why this phenomenon occurs. An explanation for this could be that the reduction in lattice vibration is not significant enough to increase conductivity. It could also be that the significant number of

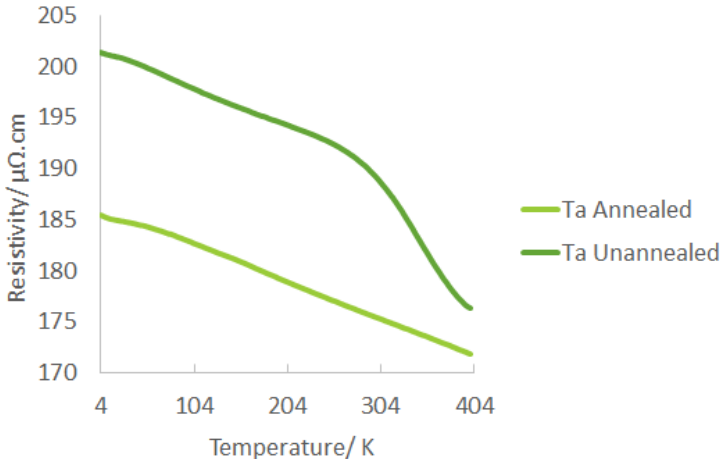

Figure 36) Resistivity measurements of as-deposited and annealed β- Ta films as a function of temperature

defects in the Ta films interstitial atoms prevent free movement of electrons even at lower temperatures. Any structural changes could also attribute to this behavior. Further studies on the microstructure, specifically lateral grain size, would help determine whether the increasing resistivity is due to electron scattering at the grain boundaries [47].

The resistivity measurements for 18% N_2: Ar, 23% N_2: Ar and 27% N_2: Ar are shown below. The samples with higher N_2: Ar ratios were extremely insulating even at room temperature (10^4-10^9 μΩ.cm) and did not yield stable measurements from the PPMS.

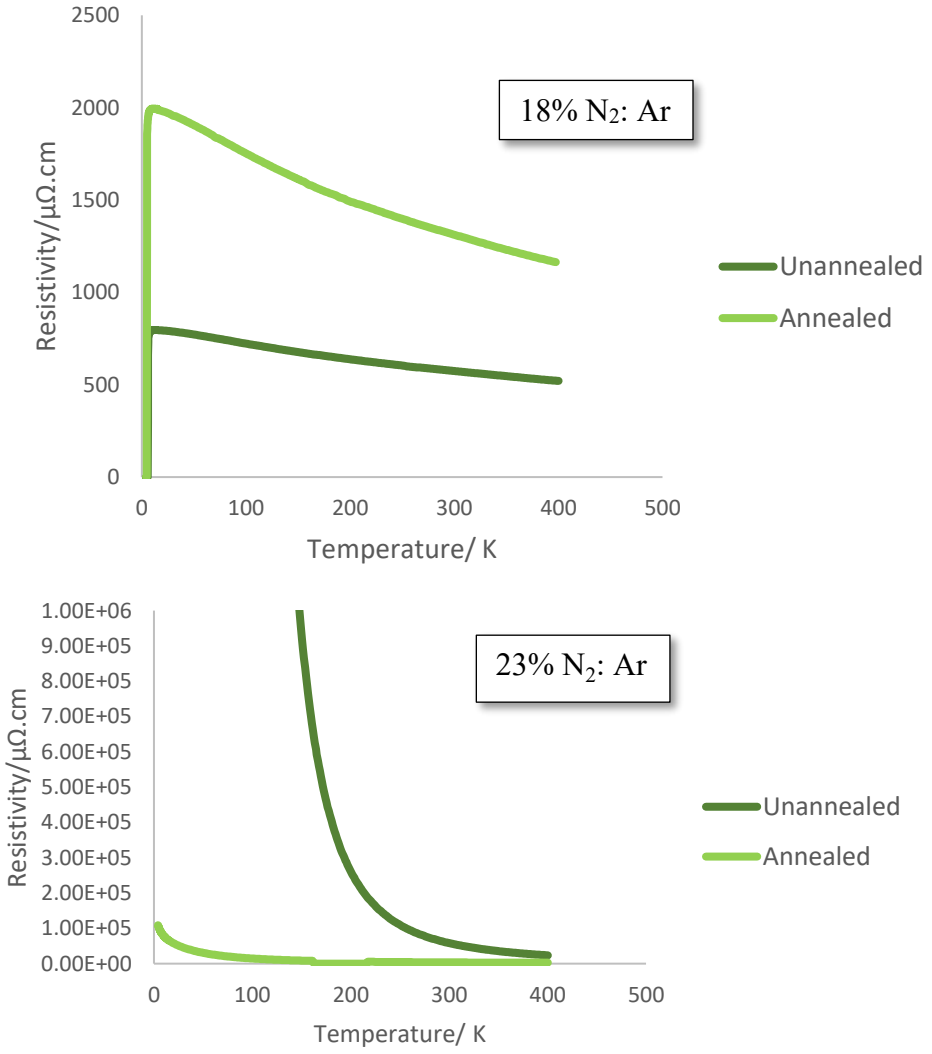

Figure 37 a) Resistivity measurements of as-deposited and annealed TaN films as a function of temperature

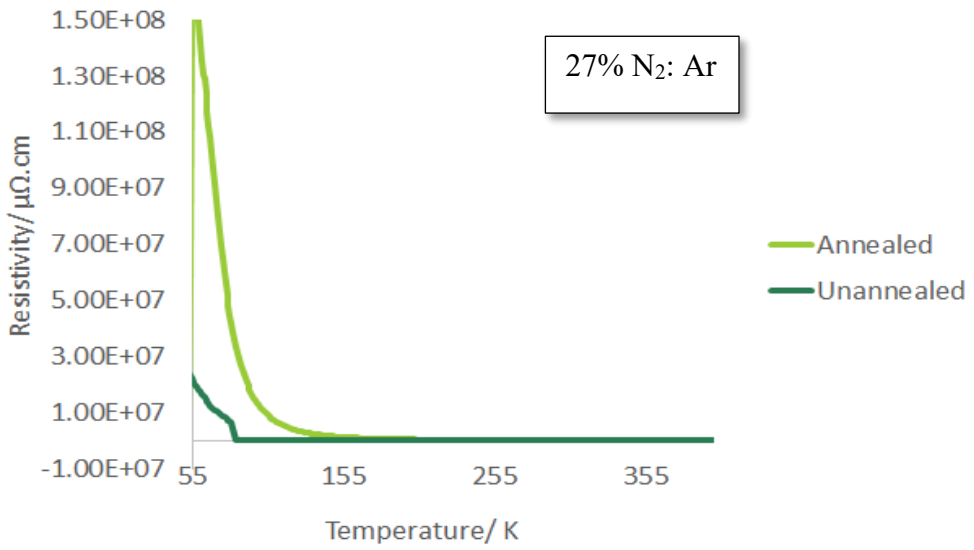

Figure 37 b) Resistivity measurements of as-deposited and annealed TaN films (27% N_2: Ar) as a function of temperature

Figure 37 shows that resistivity of films increases significantly with increase N_2 partial pressure. The resistivity of rock-salt structure TaN is seen to vary from metal to insulator as N content increases in literature [48], consistent with this study.

In N-rich conditions, the dominance of Ta vacancies was predicted to be the contributing factor towards the increased resistivity of higher N_2: Ar flow deposition ratios. The N atoms occupying the increased vacancies could be the cause for this change in electrical behavior. Thermodynamically stable phase formation (tetragonal Ta_4N_5 or orthorhombic Ta_3N_5) under N-rich conditions has been observed (as later discussed in GADDS measurements) which have higher resistivity than cubic TaN films produced from lower N_2: Ar ratios [48]. TaN films in this study, with N_2: Ar ratio of more than 27% have high resistivity and therefore could be used in GMR sensor for data storage as a seeding layer. The low-resistive

stoichiometric TaN can be used as a barrier layer for semiconductors, but the change in resistivity at lower temperatures should be taken into consideration when designing devices.

Sample	N_2: Ar/ %	Room Temperature Resistivity/ μΩ.cm
Ta_SiN	0	192
Ta_SiN_A	0	175
TaN1_SiN	18	572
TaN1_SiN_A	18	1320
TaN2_SiN	23	57900
TaN2_SiN_A	23	3560
TaN3_SiN	27	600
TaN3_SiN_A	27	83200

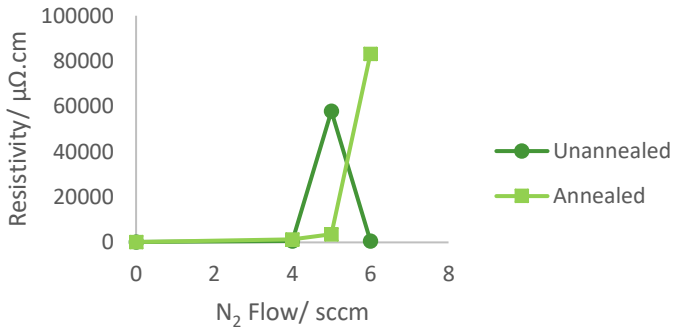

Figure 38) Room temperature resistivity trend of as-deposited and annealed TaN films as a function of temperature

There is no trend in the resistivity when the films are annealed. While some films exhibit increased resistivity from annealing (18% and 27% N_2: Ar), some decrease in resistivity as expected from annealing treatment (23% N_2: Ar). The increase from annealing may be from the N_2 anneal being at atmospheric pressure where the vacancies in TaN are filled with N atoms. It may also be due to oxidation around the grain boundaries. This is further supported by the transparency of the 82% N_2: Ar film. Figure 38 on previous page shows the trend in

room temperature resistivity for the 4 film samples shown in figure 36 and 37. No specific trend is seen in room temperature resistivity for these films, although the effect of annealing is seen to have drastically increased with increased N_2 flow. Again, this can be attributed to the generated vacancy sites with N-rich conditions and annealing in N_2 having a slightly increased effect on N-rich deposited films.

GADDS for Crystallographic Phase Identification and Texture Analysis

GADDS measurements were performed on all samples to identify phases and structural changes as the N_2: Ar ratio is increased during film deposition. As mentioned above, the structural changes can lead to change in electrical and thermal resistivity, coefficient for thermal expansion, and specific heat capacity as a result of changes in APF (atomic packing factor). Therefore, an elaborate study of samples using the GADDS can prove to be very informative.

Figure 39 below shows the different images extracted from samples. As mentioned previously, single spots are from single crystals, which in this case is the single crystal Si substrate underneath these samples. The analytical software has a method of eliminating these substrate effects so that, during phase identification, for an intensity against 2θ pattern, only peaks from the film are shown.

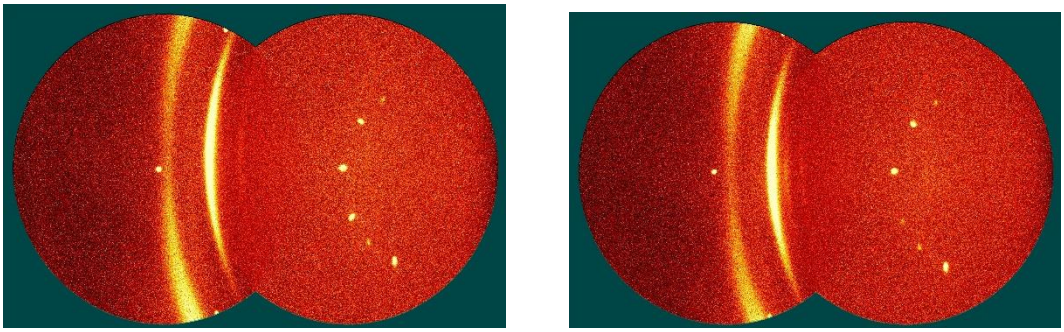

Figure 39: GADDS scans of as-deposited (left) Ta film and annealed Ta film (right)

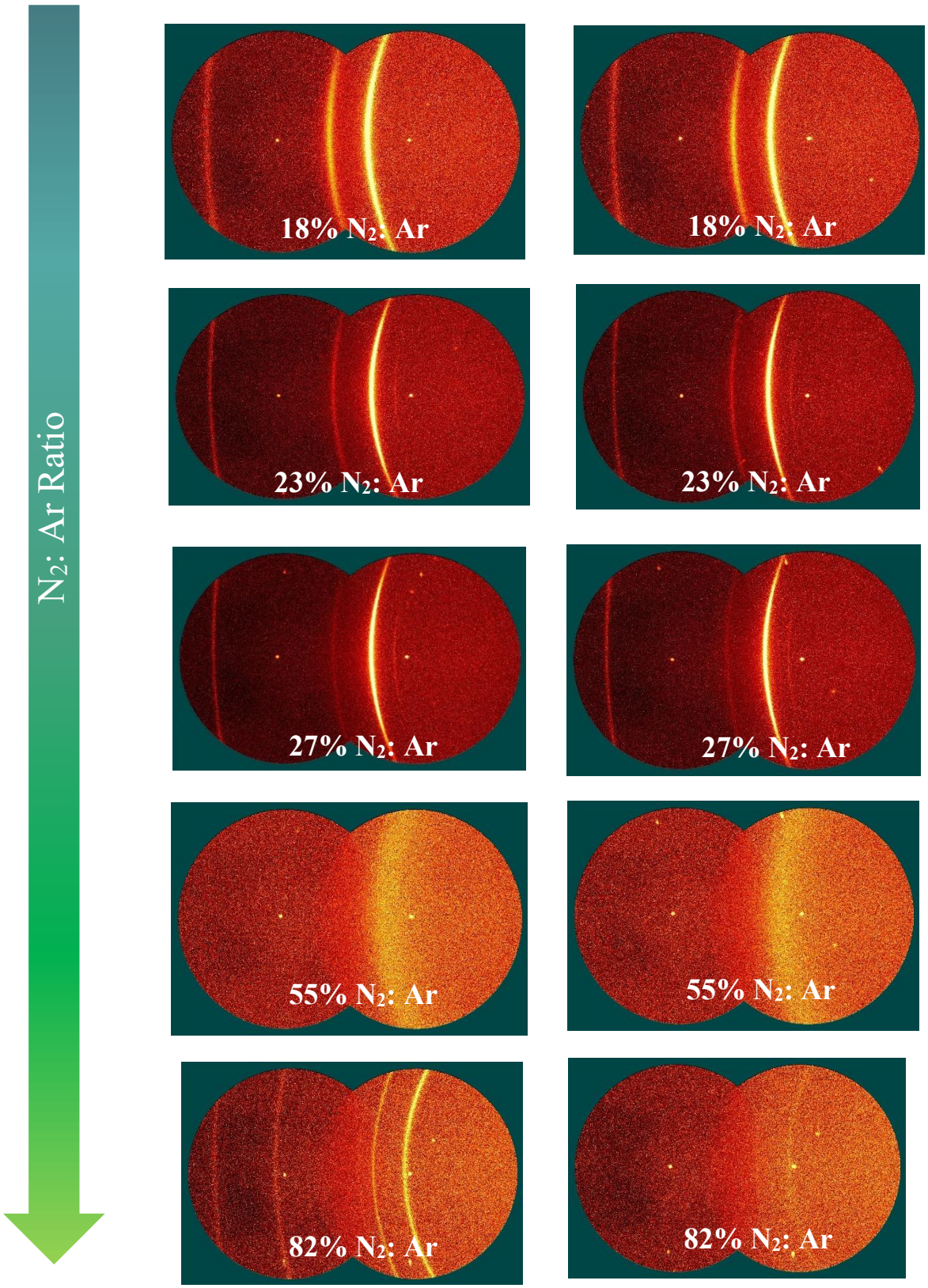

Figure 39 (continued): GADDS scans of as-deposited (left) TaN film and annealed TaN film (right)

As seen on Figure 39, annealing has no significant changes in the arcs on the GADDS scans except for the 82% N_2: Ar ratio. Additionally, the Ta film is highly textured due to the difference in arc thicknesses along the length of the arc. The 18%, 23% and 27% N_2: Ar show similar images with no significant changes observed from annealing. However, at 55% N_2: Ar, the film is amorphous. When N_2: Ar is increased further to 82%, the scans show a change in structure to be more polycrystalline and less textured. Annealing this film has also affected the structure. At lower N_2: Ar ratios, stoichiometric TaN (low resistive phase) is expected to be deposited, and, as N_2: Ar increases, more N-rich off-stoichiometric TaN phases or N-rich thermodynamically stable phases (tetragonal Ta_4N_5 and orthorhombic (Ta_3N_5) are expected to be deposited [49].

Figure 40 below shows the 2θ scans for the same samples.

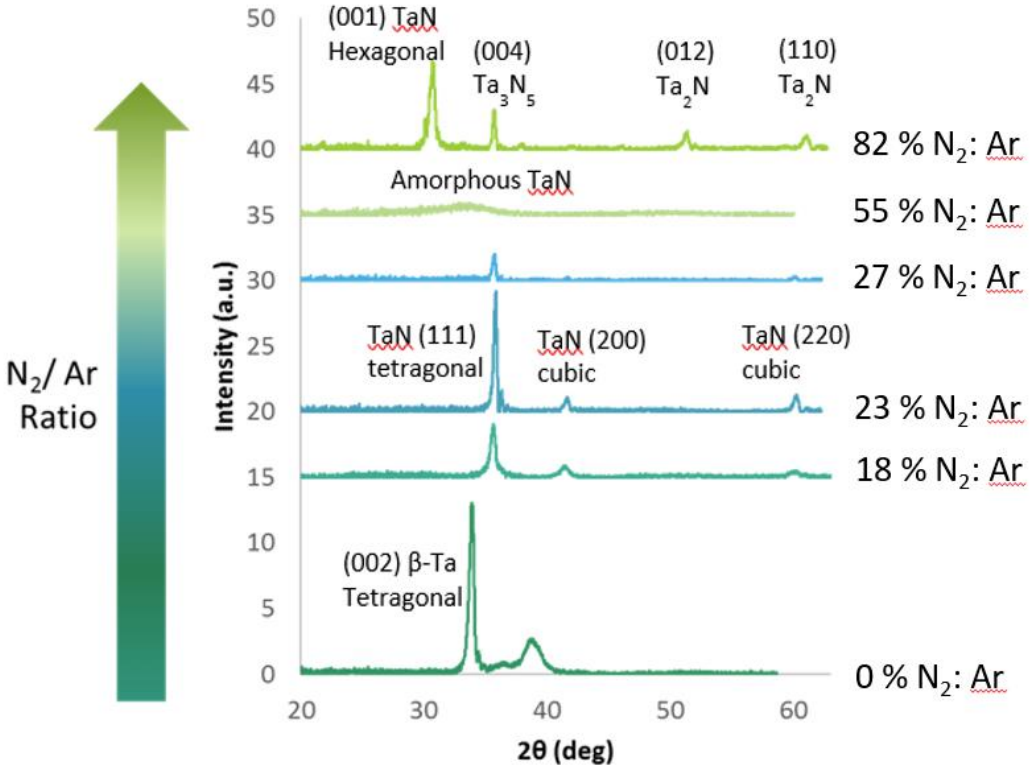

Figure 40: Pattern scans of as-deposited films [49-50]

Ta films are found to be β-phase and tetragonal from the scans shown in Figure 40 on previous page.

Similar peaks are seen in 18% N_2: Ar, 23% N_2: Ar and 27% N_2: Ar. The increased intensity in peaks for 18% N_2: Ar means that it is more crystalline and highly ordered than the 23% and 27%. Differences in crystallite sizes may lead to different intensity in respective peaks. Further studies on full width at half maximum (FWHM) using the Scherer's equation can verify further.

As the N_2 flow is further increased to 55% N_2: Ar, the film observed is amorphous. Various scans on similar samples have been done to verify the repeatability. Amorphous TaN has also been seen previously with literature [42].

Finally, the 82% N_2: Ar produces an orthorhombic Ta_3N_5 with mixed phase of hexagonal Ta_2N [49]. This thermodynamically stable phase correlates to the higher resistivity predicted for orthorhombic TaN phases [48]. More peaks over the same 2θ range, compared to other films, show more crystallinity for 82% N_2: Ar.

Flexus Film Stress Measurement Tool

The stress induced by different films are summarized in table below where positive values for stress mean tensile and negative values for stress mean compressive. Please refer to Figure 10 on page 30 for reference on definitions of tensile and compressive stress.

As discussed before, for electronic devices, the stress induced by films is preferred to be minimal to reduce surface cracking and to keep film uniformity intact.

The values on Table 4, next page, are an average of the 3 stress values (in MPa) obtained from the 3 different orientations of 0°, 45° and 90°.

Sample	N_2/ Ar %	Stress/ MPa
Ta	0	1100
TaN	18	-6
TaN	23	-210
TaN	27	-340
TaN	55	-550
TaN	82	-500

Table 4: Residual stress of thin films

The Flexus stress measurements are performed on 100nm Ta and TaN films on Si substrates with the 670nm wavelength beam.

Ta films are observed to be highly tensile whereas the minimal stress from TaN films come from 18% N_2: Ar film deposition condition. Along with the minimal stress values, this film seems to be the most ideal for electronic devices along with its stable thermal properties (specific heat capacity not changing significantly over temperature) and electrical properties (lower resistivity compared to other TaN films).

The difference in residual stresses can be attributed to the N_2 flow during deposition, as there is a clear trend between increase in amount of N_2 flow and increase in compressive stresses in the TaN. The compressive stress exhibited in tantalum films could be because of atomic peening. In such cases, the Ar and N atoms have a longer mean free path, higher momentum and with fewer collisions, brings about a compressive stress in the film [51-53].

As for the Ta film being tensile, β phase Ta and mixed phases have been developed in tensile stresses in literature whereas α phase Ta is observed to be more compressive [54].

Scanning Electron Microscopic Images of Films

SEM images were taken for every sample to ensure film uniformity and to observe significant differences in film microstructure. Although the limitations with SEM won't allow extensive study of film microstructure, further studies with cross-sectional SEM and TEM could allow further detailed studies.

Figure 41 below shows that the Ta film deposited is uniform and the roughness can also be observed.

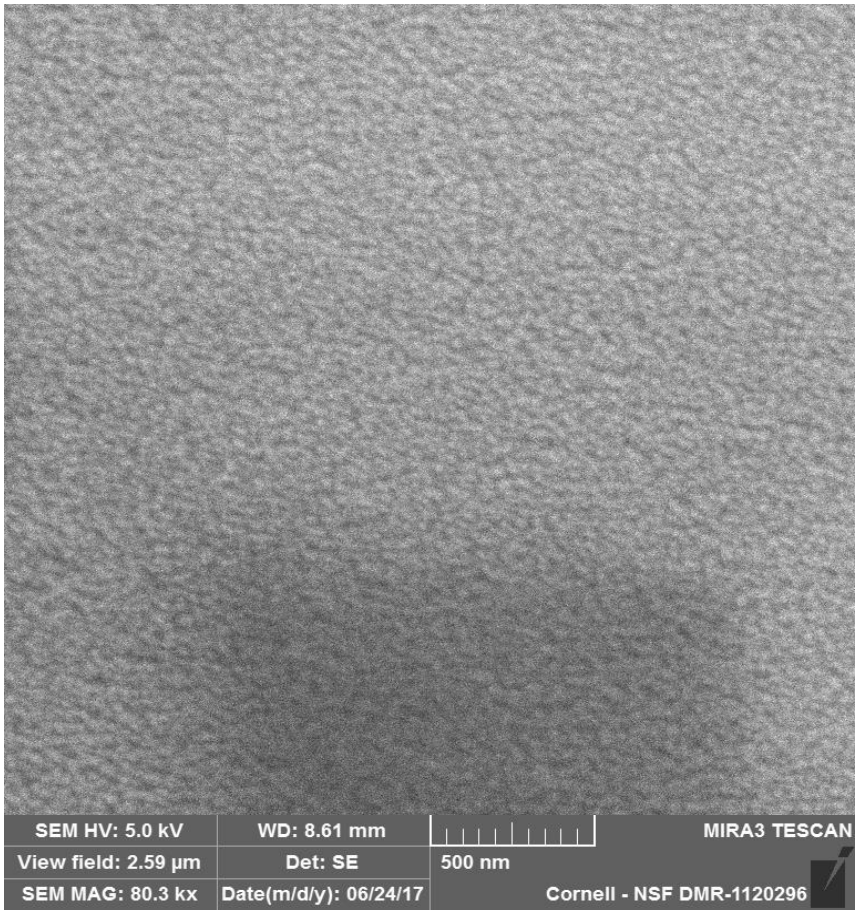

Figure 41: SEM image of 600nm Ta film on Si

Further images on other films are shown below in Figure 42.

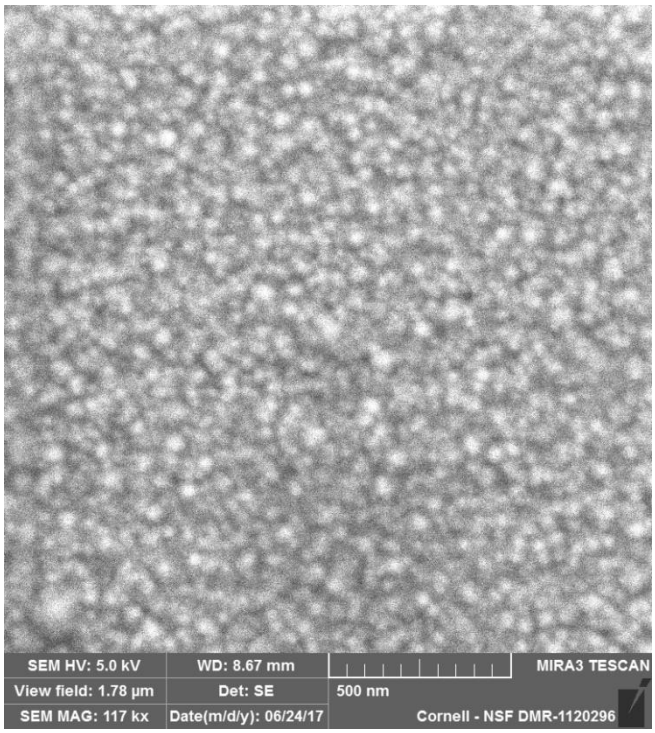

Figure 42a) SEM image of 600nm TaN (18% N_2: Ar) film on Si

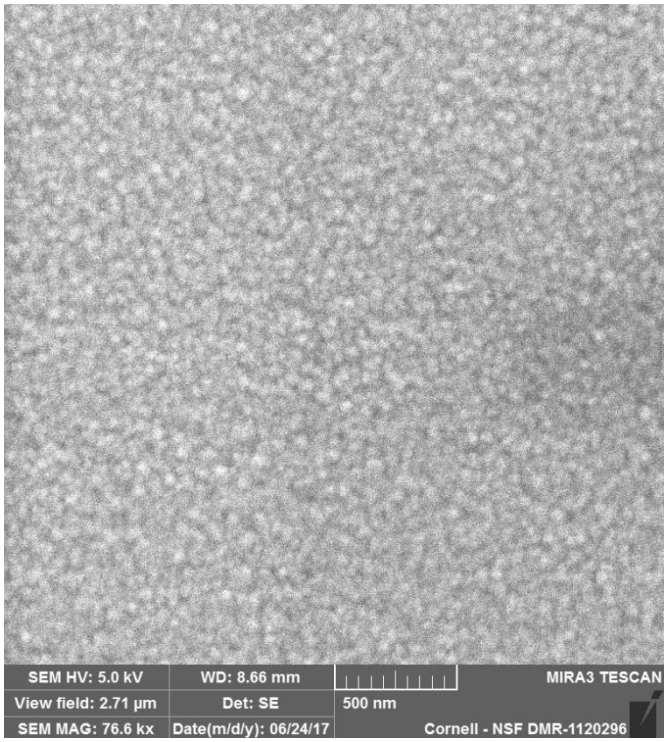

Figure 42b) SEM image of 600nm TaN (18% N_2: Ar) film on Si

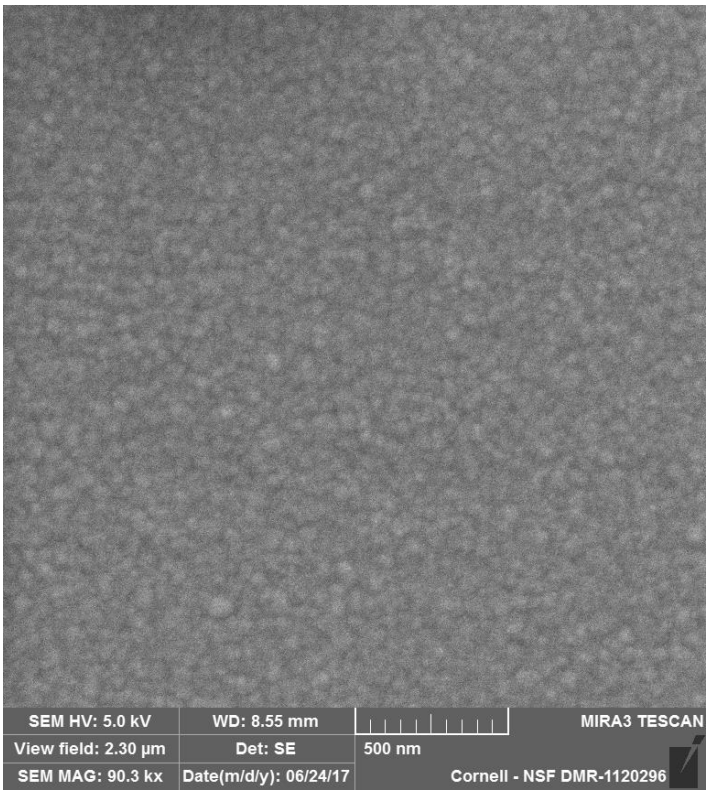

Figure 42c) SEM image of 600nm TaN (27% N_2: Ar) film on Si

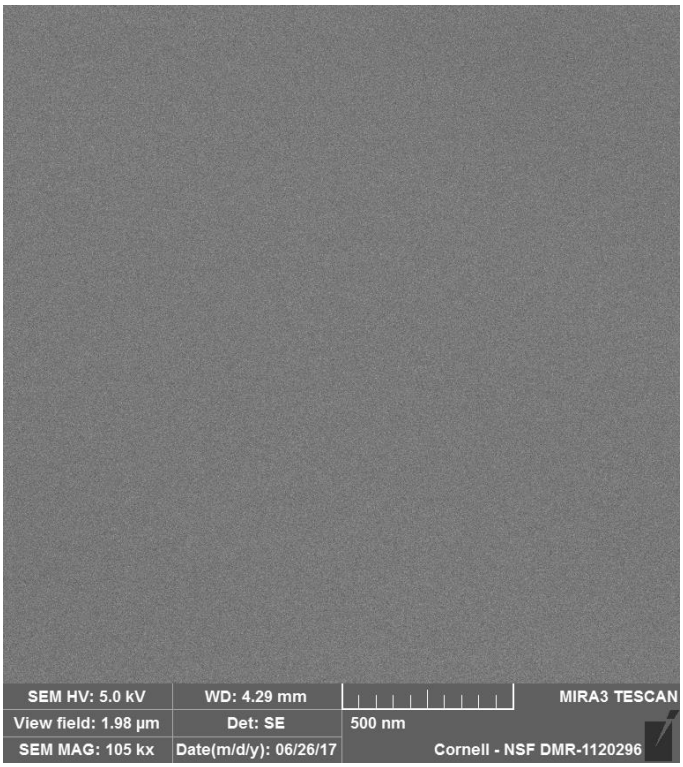

Figure 42d) SEM image of 600nm TaN (52% N_2: Ar) film on Si

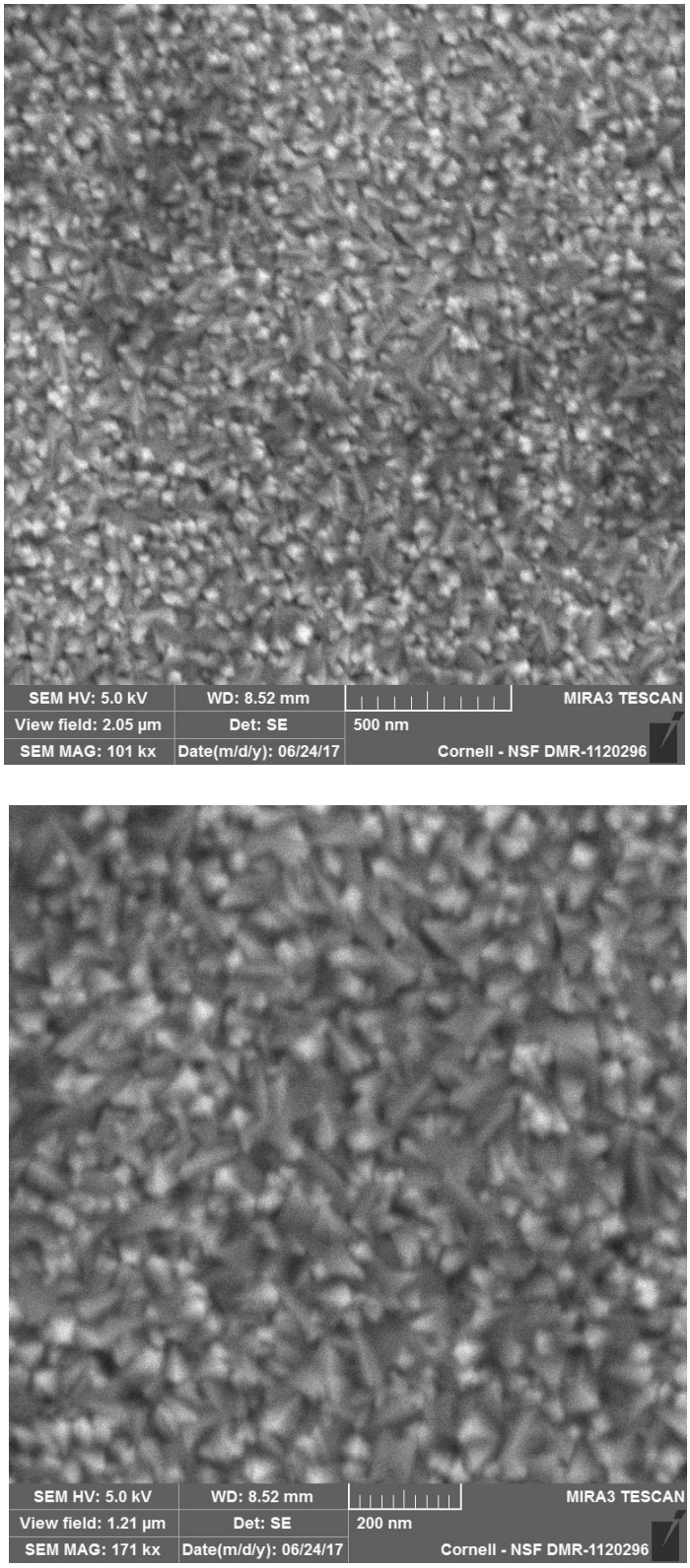

Figure 43: SEM image of 600nm TaN (82% N_2: Ar) film on Si at a) magnification of 101kx and b) 171kx

SEM images in Figure 42 further prove that the TaN films are all polycrystalline except for amorphous film on Figure 42d) for 55% N_2: Ar.

Figure 43 also shows how the N-rich films exhibit different properties and correspond to the different phase found for this film in GADDS measurements.

CHAPTER 4

CONCLUSIONS AND FUTURE WORK

Conclusions

This study includes 6 different deposition conditions when sputtering starting with pure Ta, and increasing N_2: Ar percentage from 18%, 23%, 27%, 33%, 55% and 82%. The deposition rate decreases with increased N_2: Ar ratio. The residual film stresses on substrates range from highly tensile Ta to increasingly compressive TaN with increased N_2 content. The TaN film with the lowest inducing stress was 18% N_2 with a compressive stress of -5.82 MPa. Surprisingly, limited data on the constant pressure specific heat capacity (c_p) of Ta and TaN thin films exist. It has been found that the c_p of these films increases with temperature, as seen in bulk forms of Ta and TaN. The 18% and 23% N_2 films exhibit the c_p curves closes to the bulk TaN values.

Low temperature resistivity measurements are performed using PPMS to study the effect of lattice vibrations decreasing on electrical resistivity. The electrical properties of TaN deposited in greater than 23% N_2 content, are found to be insulating, which may be a result of oxidation during slow deposition and are also observed with amorphous and orthorhombic phases in literature [48]. Annealing decreases the resistivity of Ta and TaN (23% N_2: Ar) films which is attributed to defect healing, whereas annealing increases the resistivity in the 18% and 27% N_2: Ar films which may be due to N-rich deposition conditions generating more vacancies which, in turn, are filled by N atoms during N_2 anneal. As to mechanical properties of TaN, the hardness of these films range between 10-18 GPa depending on the N_2 to Argon (Ar) ratio consistent with literature. It has been seen in

literature that the increased N_2 content gives rise to increased hardness up to about 50% N_2 and falls thereafter [13]. Vacuum annealing TaN films has also shown increased hardness which is attributed to an effect from enhanced film density [14]. The Young's modulus (E) of TaN films ranges from 150-250 GPa also consistent with literature [15]. Vacuum annealing has also shown to increase the E of these thin films, attributing this behavior to a decrease in defect concentration [14].

Additionally, GADDS measurements show different phase mixtures for the N-rich TaN films with orthorhombic Ta_3N_5 which is shown to have higher resistivity than cubic TaN and hexagonal Ta_2N. The 55% N_2: Ar exhibits an amorphous phase, consistent with SEM images. Additionally, SEM images show uniform film deposition from sputtering. It also shows the polycrystalline behavior of the films.

Future Work

Further studies on microstructure through cross-sectional SEM and TEM could prove useful in understanding the phenomena for specific heat capacity, stress and electrical measurements.

High volume DSC pans could ensure a more reliable heat flow signal from the DSC instrument as it would ensure that the minimum mass of 20mg for inorganics is met.

To eliminate the possibility of oxidation occurring during N_2 anneal, other annealing processes at lower pressures and more inert atmospheres can be made. Annealing temperatures and time could also be varied to study the effect of each variable on film properties and structural changes.

Further research on bulk materials ordered could prove useful when comparing with literature and experimental thin film values. Phase studies, EDS for exact material composition, and X-ray Photoelectron Spectroscopy (XPS) are some options.

More importantly, XPS needs to be performed on the deposited TaN films to calculate the exact N_2 content in films. Ellipsometry measurements may also prove useful by extracting refractive indices and comparing with literature, especially for films at higher N_2 flows which produced almost transparent films, which is not common in pure TaN.

Finally, DSC measurements with different heating rates can be measured such as 2K/ min and 5K/ min to study the exact changes in c_p in response to temperature.

REFERENCES

1. Kumar, Mukesh, Rajkumar, Dinesh Kumar, and A.k. Paul. *"Thermal Stability of Tantalum Nitride Diffusion Barriers for Cu Metallization Formed Using Plasma Immersion Ion Implantation." Microelectronic Engineering* 82.1 (2005): 53-59. Web.

2. Ghandhi, Sorab Khushro. *VLSI Fabrication Principles: Silicon and Gallium Arsenide*. New York: Wiley, 1983. Print.

3. Kim, Deok-Kee, Heon Lee, Donghwan Kim, and Young Keun Kim. "*Electrical and Mechanical Properties of Tantalum Nitride Thin Films Deposited by Reactive Sputtering." Journal of Crystal Growth* 283.3-4 (2005): 404-08. Web.

4. Siddiqui, Jamil, Tousif Hussain, Riaz Ahmad, Waris Ali, Ali Hussnain, and Rana Ayub. *"Growth and Study of Plasma Assisted Nanostructured Hard Tantalum Nitride Thin Films." Journal of Fusion Energy* 34.5 (2015): 1193-202. Web.

5. Han, Jeong Hwan, Hyo Yeon Kim, Sang Chan Lee, Da Hye Kim, Bo Keun Park, Jin-Seong Park, Dong Ju Jeon, Taek-Mo Chung, and Chang Gyoun Kim. *"Growth of Tantalum Nitride Film as a Cu Diffusion Barrier by Plasma-enhanced Atomic Layer Deposition from Bis((2-(dimethylamino)ethyl)(methyl)amido)methyl(tert-butylimido)tantalum Complex." Applied Surface Science* 362 (2016): 176-81. Web.

6. Liu, X., G.j. Ma, G. Sun, Y.p. Duan, and S.h. Liu. *"Effect of Deposition and Annealing Temperature on Mechanical Properties of TaN Film." Applied Surface Science* 258.3 (2011): 1033-037. Web.

7. Petrović, R., T. Nenadović, N. Kraljević, and T. Dimitrijević. *"Electrical and Structural Properties of Tantalum Nitride Thin Films Deposited by Sputtering." Thin Solid Films* 57.2 (1979): 333-36.

8. N. D. Miloševic, G. S. Vuković, D. Z. Pavičić, K. D. Maglić. *"Thermal Properties of Tantalum between 300 and 2300K".* International Journal of Thermophysics (1999) 20: 1129. doi:10.1023/A:1022659005050.

9. *"Springer Handbook of Condensed Matter and Materials Data."* Google Books. N.p.470, n.d. Web. 15 May 2017.

10. Yu, Tang Zhen-An, Zhang Feng-Tian, Wei Guang-Fen, and Wang Li-Ding. *"Investigation of a Microcalorimeter for Thin-Film Heat Capacity Measurement."* Chinese Physics Letters 22.9 (2005): 2429-432.

11. Petit, A.-T.; Dulong, P.-L. (1819). *"Recherches sur quelques points importants de la Théorie de la Chaleur"*. Annales de Chimie et de Physique (in French). 10: 395–413

12. Nie, H.b., S.y. Xu, S.j. Wang, L.p. You, Z. Yang, C.k. Ong, J. Li, and T.y.f. Liew. *"Structural and Electrical Properties of Tantalum Nitride Thin Films Fabricated by Using Reactive Radio-frequency Magnetron Sputtering."* Applied Physics A Materials Science & Processing 73.2 (2001): 229-36.

13. Grosser, M., M. Münch, H. Seidel, C. Bienert, A. Roosen, and U. Schmid. *"The Impact of Substrate Properties and Thermal Annealing on Tantalum Nitride Thin Films."* Applied Surface Science 258.7 (2012): 2894-900.

14. Riekkinen, T., J. Molarius, T. Laurila, A. Nurmela, I. Suni, and J.k Kivilahti. *"Reactive Sputter Deposition and Properties of Ta_xN Thin Films."* Microelectronic Engineering 64.1-4 (2002): 289-97.

15. Kushnir, A.j., and W. Worobey. *"Electrical Resistance as a Function of Temperature in Pure and Doped Beta-tantalum Films."* Thin Solid Films 23.2 (1974): 195-203.

16. Stella, Kevin, Damian Bürstel, Steffen Franzka, Oliver Posth, and Detlef Diesing. *"Preparation and Properties of Thin Amorphous Tantalum Films Formed by Small E-beam Evaporators."* Journal of Physics D: Applied Physics 42.13 (2009): 135417.

17. Bernoulli, D., U. Müller, M. Schwarzenberger, R. Hauert, and R. Spolenak. "*Magnetron Sputter Deposited Tantalum and Tantalum Nitride Thin Films: An Analysis of Phase, Hardness and Composition.*" Thin Solid Films 548 (2013): 157-61.

18. Moody, N. R., D. Medlin, and D. P. Norwood. *"Fracture of Thin Tantalum Nitride Films on Ain Substrates."* MRS Proceedings 436 (1996): n. pag.

19. Saha, Ranjana, and John A. Barnard. *"Effect of Structure on the Mechanical Properties of Ta and Ta(N) Thin Films Prepared by Reactive DC Magnetron Sputtering."* Journal of Crystal Growth 174.1-4 (1997): 495-500.

20. Barbés, Benigno, Ricardo Páramo, Eduardo Blanco, María José Pastoriza-Gallego, Manuel M. Pińeiro, José Luis Legido, and Carlos Casanova. "*Thermal Conductivity and Specific*

Heat Capacity Measurements of Al_2O_3 Nanofluids." Journal of Thermal Analysis and Calorimetry 111.2 (2012): 1615-625. Web.

21. Debye, Peter (1912). "*Zur Theorie der spezifischen Wärme*". Annalen der Physik (in German). Leipzig. 39 (4): 789–839. Bibcode:1912AnP...344..789D. doi:10.1002/andp.19123441404

22. Hill, T. L. An Introduction to Statistical Thermodynamics. New York: Dover, 1986.

23. K. D. Maglić, N. Lj. Perović, and G. S. Vuković, High Temp.-High Press. 29:97 (1997).

24. D. Maglić, N. Lj. Perović, Lj. P. Zeković, and G. S. Vuković, Inl. J. Thermophys.15:963 (1994).

25. A. M. Stanimirović, G. S. Vuković, and K. D. Maglić, Int. J. Thermophys. 20:325 (1999).

26. G. C. Lowenthal, Aust. J. Phys. 16:47 (1963).

27. N. S. Rasor and J. D. McClelland, J. Chem. Phys. Solids 15:17 (1959).

28. Hainsworth, S. V., H. W. Chandler, and T. F. Page. *"Analysis of Nanoindentation Load-displacement Loading Curves."* Journal of Materials Research 11.08 (1996): 1987-995.

29. Frank, Stephan, Ulrich A. Handge, Sven Olliges, and Ralph Spolenak. *"The Relationship between Thin Film Fragmentation and Buckle Formation: Synchrotron-based in Situ Studies and Two-dimensional Stress Analysis."* Acta Materialia 57.5 (2009): 1442-453.

30. Moody, N.r., R.q. Hwang, S. Venka-Taraman, J.e. Angelo, D.p. Norwood, and W.w. Gerberich. *"Adhesion and Fracture of Tantalum Nitride Films."* Acta Materialia 46.2 (1998): 585-97.

31. Jha, Kaushal K., Nakin Suksawang, Debrupa Lahiri, and Arvind Agarwal. *"A Novel Energy-based Method to Evaluate Indentation Modulus and Hardness of Cementitious Materials from Nanoindentation Load-displacement Data."* Materials and Structures 48.9 (2014): 2915-927.

32. University of Nebraska-Lincoln | Web Developer Network. "Hysitron Nanoindenter." Hysitron Nanoindenter | BM³ Facility | University of Nebraska–Lincoln. N.p., n.d. Web. 01 June 2017.

33. Oliver, W.C., and G.M. Pharr. *"An Improved Technique for Determining Hardness and Elastic Modulus Using Load and Displacement Sensing Indentation Experiments*." Journal of Materials Research" 7.06 (1992): 1564-583.

34. Alan I. Goldman, Tai Kong, Andreas Kreyssig, Anton Jesche, Mehmet Ramazanoglu, Kevin W. Dennis, Sergey L. Bud'ko, and Paul C. Canfield, "*A Family of Binary Magnetic Icosahedral Quasicrystals Based on Rare Earths and Cadmium*", Nature Materials, 2013, 12, 714-718. http://dx.doi.org/10.1038/NMAT3672

35. Moore, Lesley E.; Smart, Elaine A. (2005). Solid State Chemistry: An Introduction (3rd ed.). Boca Raton, FL: Taylor & Francis, CRC. p. 8. ISBN 0748775161

36. Ellis, Arthur B.; et al. (1995). Teaching General Chemistry: A Materials Science Companion (3rd ed.). Washington, DC: American Chemical Society. ISBN 084122725X

37. *"Current-induced surface roughness reduction in conducting thin films,"* Lin Du, Dimitrios Maroudas. Applied Physics Letters March 7, 2017. DOI: 10.1063/1.4977024.

38. R. Kuroda, T. Suwa, A. Teramoto, R. Hasebe, S. Sugawa and T. Ohmi, IEEE T-ED, Vol. 56, pp. 291-298, (2009).

39. Bhushan, B., Modern Tribology Handbook, Vol. 1 - Principles of Tribology, (2001).

40. *"Measuring Surface Roughness with Atomic Force Microscopy."* Asylum Research. Oxford Instruments, n.d. Web. 2 July 2017.

41. "*Selecting a Sample Pan*." DSC Online Help. NTNU, n.d. Web. 2 July 2017.

42. Schwartz, Newton, W.a. Reed, P. Polash, and Mildred H. Read. "*Temperature Coefficient of Resistance of Beta-tantalum Films and Mixtures with B.c.c.-tantalum."* Thin Solid Films 14.2 (1972): 333-46.

43. Salamon, K., N. RadiÄ, I. BogdanoviÄ RadoviÄ, and M. OÄko. *"Phase Map, Composition and Resistivity of Reactively Magnetron Sputtered and Annealed TaN Films*." Journal of Physics D: Applied Physics 49.19 (2016): 195301.

44. *"Bruker D8 General Area Detector Diffraction System (GADDS)."* Cornell Center for Materials Research. Cornell University, 12 May 2017. Web. 02 July 2017. <http://www.ccmr.cornell.edu/instruments/bruker-general-area-detector-diffraction-system-gadds/>.

45. Friedlander, ByBlaine. "*Making Electric Energy Efficient at Bargain Prices| Cornell Chronicle".* Cornell Nanoscale Facility, 04 Nov. 2013. Web. 02 July 2017. http://news.cornell.edu/stories/2013/11/making-electric-energy-efficient-bargain-prices

46. Mendizabal, L., R. Bayón, E. G-Berasategui, J. Barriga, and J.j. Gonzalez. *"Effect of N_2 Flow Rate on the Microstructure and Electrochemical Behavior of TaN_x Films Deposited by Modulated Pulsed Power Magnetron Sputtering."* Thin Solid Films 610 (2016): 1-9

47. Javed, A., Hina G. Durrani, and C. Zhu. "*The Effect of Vacuum Annealing on the Microstructure, Mechanical and Electrical Properties of Tantalum Films."* International Journal of Refractory Metals and Hard Materials 54 (2016): 154-58.

48. L. Yu, C. Stampfl, D. Marshall, T. Eshrich, V. Narayanan,J.M. Rowell, N. Newman, A.J. Freeman, Phys. Rev. B 65 (2002) 245110.

49. Shen, Longhai, and Nan Wang. *"Effect of Nitrogen Pressure on the Structure of Cr-N, Ta-N, Mo-N, and W-N Nanocrystals Synthesized by Arc Discharge."* Journal of Nanomaterials 2011 (2011): 1-5

50. Alishahi, M., F. Mahboubi, S. M. Mousavi Khoie, M. Aparicio, E. Lopez-Elvira, J. Méndez, and R. Gago. "*Structural Properties and Corrosion Resistance of Tantalum Nitride Coatings Produced by Reactive DC Magnetron Sputtering."* RSC Adv. 6.92 (2016): 89061-9072.

51. D.W. Hoffman, J.A. Thornton, *Internal stresses in Cr, Mo, Ta, and Pt filmsdeposited by sputtering from a planar magnetron source*, J. Vac. Sci. Technol.20 (3) (1982) 355–358.

52. J.A. Thornton, D.W. Hoffman, *Internal stresses in titanium, nickel,molybdenum, and tantalum films deposited by cylindrical magnetronsputtering*, J. Vac. Sci. Technol. 14 (1) (1977) 164–168

53. H. Windischmann, *Intrinsic stress in sputter-deposited thin-films*, Crit. Rev.Solid State 17 (6) (1992) 547–596.

54. A.A. Navid, A.M. Hodge. "*Controllable residual stresses in sputterednanostructured alpha-tantalum".* Scr. Mater. 63 (8) (2010) 867–870.

55. Chung, C.k., and T.s. Chen. *"Effect of Microstructures on the Electrical and Optoelectronic Properties of Nanocrystalline Ta-Si-N Thin Films by Reactive Magnetron Cosputtering." Scripta Materialia* 57.7 (2007): 611-14.

56. Petit, A.-T.; Dulong, P.-L. (1819). "*Recherches sur quelques points importants de la Théorie de la Chaleur"*. Annales de Chimie et de Physique (in French). **10**: 395–413